Copy 319
RM L50K29

NACA

RESEARCH MEMORANDUM

LOW-SPEED LONGITUDINAL AND WAKE AIR-FLOW

CHARACTERISTICS AT A REYNOLDS NUMBER OF 6.0×10^6 OF

A 52° SWEPTBACK WING EQUIPPED WITH VARIOUS SPANS OF

LEADING-EDGE AND TRAILING-EDGE FLAPS, A FUSELAGE, AND

A HORIZONTAL TAIL AT VARIOUS VERTICAL POSITIONS

By Roland F. Griner and Gerald V. Foster

Langley Aeronautical Laboratory
Langley Field, Va.

NATIONAL ADVISORY COMMITTEE
FOR AERONAUTICS
WASHINGTON
February 28, 1951

NATIONAL ADVISORY COMMITTEE FOR AERONAUTICS

RESEARCH MEMORANDUM

LOW-SPEED LONGITUDINAL AND WAKE AIR-FLOW

CHARACTERISTICS AT A REYNOLDS NUMBER OF 6.0×10^6 OF

A 52° SWEPTBACK WING EQUIPPED WITH VARIOUS SPANS OF

LEADING-EDGE AND TRAILING-EDGE FLAPS, A FUSELAGE, AND

A HORIZONTAL TAIL AT VARIOUS VERTICAL POSITIONS

By Roland F. Griner and Gerald V. Foster

SUMMARY

Investigations have been conducted in the Langley 19-foot pressure tunnel to determine the effects of extensible leading-edge flaps on the low-speed static longitudinal stability characteristics of a 52° swept-back wing which had NACA 64_1-112 airfoil sections and an aspect ratio of 2.88. Leading-edge-flap spans of 25, 35, 40, and 45 percent wing semispan were investigated and some of the more satisfactory configurations were further investigated with various combinations of trailing-edge flaps, fences, a fuselage, and a horizontal tail. Surveys of the air flow behind the wing at approximately the location of a horizontal tail were made for wing-fuselage combinations both with and without 0.40-semispan leading-edge and trailing-edge flaps. The tests were made at a Reynolds number of 6.0×10^6 and a Mach number of 0.12.

The addition of leading-edge flaps which extended over the outer 25, 35, 40, or 45 percent of the wing semispan improved the longitudinal stability characteristics of the wing through the lift range but had only a small effect on the maximum lift coefficient of the wing (1.12). From a stability consideration, either the 0.40-semispan or the 0.45-semispan leading-edge flaps were optimum depending on the trailing-edge-flap configuration.

The extended trailing-edge flaps were a considerably more effective means of increasing the lift coefficient of the wing throughout the angle-of-attack range than were the split flaps.

The most favorable longitudinal stability characteristics and maximum-lift-coefficient results were obtained with 0.50-semispan extended trailing-edge flaps in conjunction with 0.40-semispan leading-edge flaps. With the 0.40-semispan leading-edge flaps, the wing was stable and had a maximum lift coefficient of 1.19. The addition of the 0.50-semispan extended trailing-edge flaps provided a maximum lift coefficient of 1.36 and the stability was maintained throughout the lift range.

The fuselage decreased the stability near maximum lift coefficient of the configuration with 0.40-semispan leading-edge flaps. The destabilizing effect of the fuselage was not obtained for configurations with fences or with 0.25-semispan leading-edge flaps.

In the high angle-of-attack range, the tail located below the wing-chord plane extended is below the wake and in a region where the rate of change of downwash with angle of attack is stabilizing. Tail positions above the wing-chord plane extended are either in or above the wake and are adversely affected by the rate of change of downwash with angle of attack. In general, stability was obtained throughout the angle-of-attack range for configurations with the tail located below the wing-chord plane extended; whereas, for most configurations with the tail located above the wing-chord plane extended, instability or a very small degree of stability was obtained in the high angle-of-attack range.

INTRODUCTION

The undesirable low-speed static longitudinal stability characteristics associated with sweptback wings have frequently been alleviated by delaying the tip stall (reference 1) or diffusing the leading-edge vortex flow (reference 2) by the use of leading-edge flaps.

In an attempt to improve the longitudinal characteristics of a 52° sweptback wing reported in reference 3, leading-edge flaps which extended over the outer 57.5 percent of wing semispan were found to be only partially satisfactory. It was found that trailing-edge flaps and upper-surface fences were also necessary in order to obtain satisfactory longitudinal stability characteristics in the high-lift range (reference 4). Tests of other swept wings have since revealed the critical dependency of longitudinal stability characteristics on the span of leading-edge flaps (references 2 and 5). In view of this fact, it was believed that the longitudinal stability characteristics of the 52° sweptback wing with leading-edge flaps of shorter spans than heretofore considered might be satisfactory without the use of other devices.

    The present paper presents the results of low-speed tests in the Langley 19-foot pressure tunnel at Reynolds number of 6.0×10^6 of a $52°$ sweptback wing with leading-edge flaps of 25, 35, 40, and 45 percent wing semispan. In addition, results are presented which show the effect of 40- and 50-percent-wing-semispan trailing-edge flaps, a fuselage, and a horizontal tail on the longitudinal characteristics of the wing with the span of leading-edge flaps which appeared optimum from the standpoint of stability. To assist in evaluating the contribution of the horizontal tail to the stability of the wing-fuselage combination, airflow surveys were made behind the wing at approximately the location of a horizontal tail.

<div align="center">SYMBOLS</div>

C_L lift coefficient (L/qS)

$C_{L_{max}}$ maximum lift coefficient

C_D drag coefficient $\left(\dfrac{D}{qS}\right)$

C_m pitching-moment coefficient, moment about the quarter chord of mean aerodynamic chord $\left(\dfrac{\text{Pitching moment}}{q\bar{c}S}\right)$

L lift, pounds

D drag, pounds

S area (wing area unless otherwise noted), square feet

$\bar{c}$ mean aerodynamic chord measured parallel to the plane of symmetry, feet $\left(\dfrac{2}{S}\displaystyle\int_0^{b/2} c^2\,dy\right)$

b span (wing span unless otherwise noted), feet

c local chord, (wing chord unless otherwise noted), feet

y spanwise ordinate, feet

z vertical distance, feet

q free-stream dynamic pressure, pounds per square foot $\left(\dfrac{\rho V^2}{2}\right)$

ρ mass density of air, slugs per cubic foot

α angle of attack of wing chord, degrees

$\alpha_{C_{L_{max}}}$ angle of attack of wing chord at $C_{L_{max}}$, degrees

V free-stream velocity, feet per second

R Reynolds number

τ tail stability parameter $\left(\dfrac{dC_{m_t}}{d\alpha}\dfrac{1}{C_{L_{\alpha_t}}\dfrac{l}{\bar{c}}\dfrac{S_t}{S}}\right)$

$C_{L_{\alpha_t}}$ lift-curve slope of isolated tail (0.0495 per degree)

$\dfrac{q_t}{q}$ ratio of local dynamic pressure to free-stream dynamic pressure (unless otherwise noted)

ϵ local downwash angle (unless otherwise noted), degrees

σ local sidewash angle, degrees, inflow negative

$C_{m_{i_t}}$ tail effectiveness parameter $\left(\dfrac{dC_m}{di_t}\right)$

$\left(C_{m_{i_t}}\right)_o$ value of $\dfrac{dC_m}{di_t}$ at zero lift for a given tail position and configuration

$\left(C_{m_{i_t}}\right)_o'$ value of $\dfrac{dC_m}{di_t}$ at zero lift for a high tail position with flaps off

η tail efficiency factor $\left(\dfrac{\left(C_{m_{i_t}}\right)_o}{\left(C_{m_{i_t}}\right)_o'}\right)$

i_t angle of incidence of horizontal tail measured with respect
               to wing-chord plane, positive when trailing edge moves
               down, degrees

l tail length, distance in wing-chord plane from quarter-
               chord point of wing mean aerodynamic chord to quarter-
               chord point of tail mean aerodynamic chord, feet

Λ sweep angle, degrees

A aspect ratio

$\dfrac{dW}{d\alpha}$ rate of change of wake center location (from extended
                        wing-chord plane) with angle of attack

Subscripts:

av   average

e   effective

t   horizontal tail

o   value at zero lift

MODEL AND APPARATUS

    The geometric characteristics of the model are given in figures 1
and 2. The wing had an aspect ratio of 2.88, taper ratio of 0.625, and
52.05° sweepback along the leading edges. The wing was composed of
NACA 64_1-112 airfoil sections in a plane normal to the 0.282-wing-chord
line and had no twist or dihedral.

    The extensible leading-edge flaps were deflected 50° with respect
to the wing-chord plane measured in a plane normal to the 0.282-wing-
chord line and extended inboard from 0.975b/2 to a maximum distance of
0.525b/2 (fig. 2). Provisions were made for several intermediate flap
spans which extended over the outer 25, 35, and 40 percent of the wing
semispan. These flaps had a constant chord, but in terms of local wing
chord the flaps were approximately 14 percent and 16 percent of the
local wing chords at the outboard and inboard ends.

    The wing was equipped with 20-percent-chord trailing-edge flaps
which were located at two chordwise positions as shown in figure 2.
One set of flaps located at the trailing edge of the wing are referred

to as "extended trailing-edge flaps," whereas those located at the 80-percent-chord line are referred to as "split flaps." These flaps were deflected 60° with reference to the lower surface of the wing, measured in a plane normal to the 0.282-wing-chord line.

The upper-surface fences (fig. 2) had a constant height equal to 60 percent of the maximum local airfoil thickness (as used in reference 4) and were located parallel to, and 0.65b/2 from, the model plane of symmetry.

The fuselage had a circular cross section (maximum diameter of 14.86 percent wing span) and a fineness ratio of 10.2. The profile of the fuselage is given in reference 4. The wing was attached to the fuselage in a midwing position with a positive incidence of 2° between the fuselage center line and the wing-chord plane. The junctures of the wing and fuselage were not filleted.

The horizontal tail had 42.05° sweepback at the leading edges, a taper ratio of 0.625, aspect ratio of 4.01, and NACA 0012-64 airfoil sections parallel with the plane of symmetry. The tail area was 16.8 percent of the wing area and the tail length l was 1.736 of the wing mean aerodynamic chord. The vertical location of the tail is defined as the distance measured perpendicular from the wing-chord plane to the $0.25\bar{c}_t$ point of the tail (fig. 1). The incidence of the tail is measured with reference to the wing-chord plane.

The six-tube survey rake of the Langley 19-foot pressure tunnel described in reference 6 was employed to measure local dynamic pressures, sidewash angles, and downwash angles.

                                        TESTS

        The tests were conducted in the Langley 19-foot pressure tunnel with the model mounted on the normal supports as shown in figure 3. The tunnel atmosphere was compressed to approximately 33 pounds per square inch, absolute, for the test. The tests were made at a Reynolds number of 6.0×10^6 and a Mach number of 0.12. Measurements of lift, drag, and pitching moment were made through an angle-of-attack range from approximately -4° to 31°. The wing air flow was studied by means of wool tufts attached to the upper wing surface and by means of a probe. Surveys of dynamic-pressure ratio, sidewash angle, and downwash angle, in the vicinity where a horizontal tail might be located, were made at angles of attack of 3.3°, 8.1°, 13.0°, 16.3°, 19.0°, and 23.1°. The plane of survey, 1.65 mean aerodynamic chords behind the 0.25 mean aerodynamic chord of the wing, was selected as a compromise location based on the

fore and after movement through the angle-of-attack range of 0.25 mean aerodynamic chord of the tail in the various positions. The maximum deviation of the 0.25 mean aerodynamic chord of the tail from the plane of survey occurred at the high angles of attack and amounted to about 7.0 percent of the tail length l forward and 11.5 percent of the tail length rearward.

REDUCTION OF DATA

Force and moment characteristics.- The lift, drag, and pitching-moment data presented in nondimensional coefficient form have been corrected for the effects of tares and interference of model supports. A correction for air-stream misalinement has been applied to the values of angle of attack and drag coefficients. Jet-boundary corrections based on the method presented in reference 7 have been applied to the angles of attack, drag coefficients, and pitching-moment coefficients.

Air-flow characteristics.- The jet-boundary effects applied to the air-stream survey data were an angle change to the downwash and downward displacement of the flow field with respect to the vertical survey locations in the plane of survey.

During the air-flow surveys, downwash angles were encountered which exceeded the calibration of the survey rake. Linear extrapolations of the calibration data were made in order to provide a few values of downwash angles (between 19° and 26°), sidewash, and local dynamic pressures for angles of attack between 19° and 23.1°. The inaccuracies introduced by extrapolating are believed to be relatively small.

Average values of downwash and dynamic pressure.- The average values of the dynamic-pressure ratio and the downwash angle in the region of a horizontal tail were obtained from the measured values of the air-flow surveys according to the following equations:

$$(q_t/q)_{av} = \frac{2}{S_t} \int_0^{b_t/2} \frac{q_t}{q} c_t \, dy$$

and

$$\epsilon_{av} = \frac{2}{S_t (q_t/q)_{av}} \int_0^{b_t/2} \frac{q_t}{q} \epsilon c_t \, dy$$

Effective values of downwash and dynamic pressure.- The effective values of dynamic-pressure ratio and the downwash angle are based on pitching-moment data. Because an isolated tail test (reference 8) showed a constant lift-curve slope through the angle-of-attack range, the computations of the effective dynamic-pressure ratio and the effective downwash angle were simplified to

$$\left(q_t/q\right)_e = \frac{C_{m_{i_t}}}{\left(C_{m_{i_t}}\right)_o}$$

and

$$\epsilon_e = \alpha + i_t - \alpha_t$$

where

$$\alpha_t = \frac{C_{m_t}}{C_{m_{i_t}}}$$

Tail efficiency factor.- The tail efficiency factors have been based on the rate of change of pitching moment with tail-incidence angle. It was assumed that the interference effects for the high-tail positions were negligible and that, with the flaps off, the dynamic-pressure ratio would be approximately 1.0 at zero lift for the high tail. The efficiency factor η was then obtained from the relation

$$\eta = \frac{\left(C_{m_{i_t}}\right)_o}{\left(C_{m_{i_t}}\right)_o'}$$

where the prime refers to the value for the high tail with flaps off.

It should be noted that the accuracy of the values of $\left(C_{m_{i_t}}\right)_o$ depends on the accuracy of measuring the tail incidence, the pitching moment, and also the dynamic-pressure ratio at the tail which may not

be unity at zero lift. The accuracy of the tail-incidence angle is believed to be within $\pm 0.2^\circ$ for each setting.

Tail effectiveness parameter.- The combined effects of ϵ and q_t/q on the stabilizing moment contributed by the tail can be shown by considering the stability parameter τ, which is defined as follows:

$$\tau = -\left[\left(1 - \frac{\partial \epsilon}{\partial \alpha}\right)\frac{q_t}{q} + \alpha_t \frac{\partial\left(q_t/q\right)}{\partial \alpha}\right]\eta \qquad (1)$$

where

$$\alpha_t = \alpha - \epsilon + i_t \qquad (2)$$

which is equivalent to

$$\tau = \frac{\left(dC_{m_t}/d\alpha\right)_{measured}}{\frac{S_t}{S}\frac{l}{c}C_{L_{\alpha_t}}} \qquad (3)$$

where

$$\frac{S_t}{S}\frac{l}{c}C_{L_{\alpha_t}} = 0.0144$$

When the tail is contributing stability, the sign of τ is negative.

It may be seen from equation (1) that when $\dfrac{\partial\left(q_t/q\right)}{\partial \alpha}$ is zero, the values of τ are independent of tail load and hence are applicable to any degree of trim or to any center-of-gravity location. The values of τ presented herein were obtained with a fixed tail incidence, and large out-of-trim conditions existed at the high angles of attack. Through the angle-of-attack range for which the tail passes through the

wake, finite values of $\dfrac{\partial(q_t/q)}{\partial\alpha}$ are obtained, and hence the values of τ

through that angle-of-attack range are more nearly applicable to the
center-of-gravity location at which the measured tail load would pro-
vide trim when the tail is at the center of the wake.

.It has been found that through the angle-of-attack range for which

values of $\dfrac{\partial(q_t/q)}{\partial\alpha}$ of the present wing are maximum, values of τ are

applicable to a trim condition for a center-of-gravity location rear-
ward of 25 percent $\bar{c}$. An analysis was made to determine the effects
of trim on the values of τ with the center of gravity located at

25 percent $\bar{c}$. It was found that, when values of $\dfrac{\partial(q_t/q)}{\partial\alpha}$ were signifi-

cant, the changes in α_t required to provide trim were such that the

product of these terms, $\Delta\alpha_t \dfrac{\partial(q_t/q)}{\partial\alpha}$, produced only minor effects on the

trends indicated by the variation of τ presented.

RESULTS AND DISCUSSION

Wing Configuration

Basic wing.- The aerodynamic characteristics of the wing presented
in reference 3 and figure 4 indicate that a large increase in the sta-
bility, accompanied by abrupt changes in the lift and drag character-
istics, occurred between angles of attack of approximately 13° to 18°.
At higher angles of attack the wing exhibited a nose-up pitching moment.
The initial changes of the aerodynamic characteristics have been
attributed in reference 3 to a possible increase of lift and drag near
the tips caused by a vortex flow over the tip sections of the wing.
The longitudinal instability at angles of attack greater than 18° was
attributed in reference 3 to the growth of separated flow near the tip
which decreased the relative lift load carried outboard; however, the
more extensive tuft and probe studies of the current investigation
indicate that the flow conditions are not fully described in reference 3.
In the current investigation it was observed that the leading-edge
vortex flow was not confined to the outboard part of the wing, as indi-
cated in reference 3, but extended along the entire leading edge of the
wing. A description of the vortex flow closely parallels that given in
reference 2. From the present studies the unstable break of the moment
curve at about 18° angle of attack is attributed to an inboard shift of

the lateral center of pressure caused by the effects of separated flow near the tips as well as the vortex flow on the inboard sections of the wing.

Leading-edge flaps.- The aerodynamic characteristics of the wing with various spans of leading-edge flaps are presented in figure 4 and summarized in table I. In order to show comparatively the effects of the various flap spans on the longitudinal stability characteristics of the wing, the variations of dC_m/dC_L are presented in figure 5.

The leading-edge flaps effectively prevented the large initial increase in stability of the wing between angles of attack of approximately 13° and 18°. Leading-edge flaps of 25, 35, or 45 percent wing semispan had a marked stabilizing effect at or near $C_{L_{max}}$ which was contrary to that noted for the 0.575b/2 flaps in figure 4. The prevention of the increase in the stability of the wing between angles of attack of 13° and 18° probably results from a delay of the separation over the outboard sections of the wing and a relocation of the vortex flow over the outer sections of the wing. Although the direct cause for the stabilizing effect of the leading-edge flaps at or near $C_{L_{max}}$ is not perceptible from these data, the leading-edge flaps may provide an increase of the load-carrying ability of the tip sections, which overbalances the effect of the vortex flow on the inboard sections, thereby resulting in a stable break of the pitching-moment curve. The leading-edge flap which extends over the outer 0.45b/2 provided the minimum change of dC_m/dC_L through the lift range of the wing (fig. 5); thus, this span was considered about optimum for the configuration with trailing-edge flaps off.

The effects of leading-edge flaps on the longitudinal stability characteristics of the present wing were compared with those of a circular-arc wing (reference 2) which had a nearly identical plan form and also showed the effects of a leading-edge vortex. The spans of leading-edge flaps which provided the most satisfactory longitudinal stability of the wings were different despite the identity of the plan forms. In the case of the circular-arc wing, the 0.25b/2 leading-edge flaps provided the most satisfactory improvement in the longitudinal stability and was slightly better than that obtained with the 0.45b/2 leading-edge flaps on the present wing. The difference in optimum leading-edge-flap span of these wings is attributed to the fact that the formation, strength, and position of the vortex flow, among other things, is dependent on the wing leading-edge (sharp or round) shape and radii.

The various spans of leading-edge flaps had only a small effect on the maximum lift of the wing $\left(C_{L_{max}} = 1.12\right)$. These effects are summarized in table I.

Leading-edge and trailing-edge flaps.- The addition of 0.40b/2 and
0.50b/2 trailing-edge flaps to the wing incorporating 0.45b/2 leading-
edge flaps resulted in an unstable variation of the pitching moment
(figs. 6 and 7) near $C_{L_{max}}$. The unfavorable influence of trailing-edge
flaps caused attention to be directed toward shorter spans of leading-
edge flaps which provided larger negative pitching-moment coefficients
at high angles of attack than that obtained with the 0.45b/2 leading-
edge flaps. (See fig. 4.)

The longitudinal characteristics of the wing with trailing-edge
flaps and 0.40b/2 leading-edge flaps are presented in figures 8 and 9,
in addition to the results with the trailing-edge flaps off. This span
of leading-edge flaps produced nearly the same changes in the stability
of the wing with trailing-edge flaps off as the 0.45b/2 leading-edge
flaps (fig. 10). With trailing-edge flaps on, however, the 0.40b/2
leading-edge flaps provided fairly stable variation through the C_L
range except in the case of the 0.50b/2 split flaps (fig. 10).

These flap-on results and those of reference 5 indicate that the
longitudinal stability characteristics of swept wings may be critically
dependent on the combination of the leading-edge- and trailing-edge-flap
spans.

The extended trailing-edge flaps prove a more effective means of
increasing the value of $C_{L_{max}}$ than the split flaps (table I). In the
case of the 0.40b/2-leading-edge-flap configuration, the addition of
0.50b/2 extended trailing-edge flaps increased the values of $C_{L_{max}}$
from 1.19 to 1.36. The largest value of $C_{L_{max}}$ (1.44) was obtained
with the 0.45b/2-leading-edge-flap configuration; however, near this
value of C_L the wing became unstable.

The effects of the various trailing-edge flaps on C_L in the
linear lift range of the wing with 0.40b/2 and 0.45b/2 leading-edge
flaps are summarized in the following table:

Leading-edge-flap span (b/2)	Trailing-edge flap		Increment of lift coefficient	Figure
	Type	Span (b/2)		
0.40	Split	0.40 .50	0.24 .26	8
	Extended	.40 .50	.34 .39	9
0.45	Split	.40 .50	.24 .26	6
	Extended	.40 .50	.34 .39	7

Wing-Fuselage Configuration

Horizontal tail off.- The results of tests of several wing con-
figurations equipped with a fuselage in a midwing position are presented
in figures 11 to 13. It may be seen from table I that the addition of
the fuselage to wing configurations which were stable with the fuselage
off resulted in an unstable pitching-moment variation near $C_{L_{max}}$
except for the configurations with 0.25b/2 leading-edge flaps and with
0.40b/2 leading-edge flaps and fences. In the case of the 0.25b/2-
leading-edge-flap configuration, a stabilizing change in dC_m/dC_L was
realized near $C_{L_{max}}$ similar to that previously shown for the fuselage-
off condition. Similar destabilizing effects of a fuselage have been
noted for a 42° sweptback wing (reference 1) where the maximum per-
missible span of leading-edge flaps was used; furthermore, with some-
what shorter spans of leading-edge flaps the fuselage effect became
unimportant. It should be pointed out that, in the case of another
sweptback wing of fairly large aspect ratio, the fuselage effects were
minor (reference 5). The stabilizing effect of the fences (fig. 13)
in the case of the 0.40b/2-leading-edge-flap configuration is attributed
to a rearward shift of the center of pressure which is believed to arise
from the influence of the fences on characteristics of the wing sections
outboard of the fences.

The addition of the fuselage to the plain wing caused a small
increase in $C_{L_{max}}$ but had only minor effects on the lift coefficient
throughout the linear range. In the case of the wing equipped with
leading-edge and trailing-edge flaps, the addition of the fuselage
caused an increase in the lift-curve slope for the linear lift range
and an associated loss in lift in the low angle-of-attack range. A
somewhat similar lift-curve-slope change was observed in the case of
the 42° sweptback circular-arc wing reported in reference 9.

Horizontal tail on.- The results of tests with a horizontal tail
located at various vertical positions (fig. 1) on the wing-fuselage
combination are presented in figures 14 and 15. The effects of the
horizontal tail on the longitudinal stability characteristics are
summarized in table II. The effect of the horizontal tail on the wing-
fuselage combination with 0.40b/2 leading-edge and trailing-edge flaps
is substantially the same as that reported in reference 4 where larger
spans of flaps were employed.

The tail provided a large increase in the stability (as measured
by $dC_m/d\alpha$) through the low and moderate lift range. This stabilizing
effect decreased when the tail was moved from 0.504b/2 above to

0.074b/2 below the extended wing–chord plane (fig. 14). The difference
in the stability obtained with the tail in various positions is associated
primarily with an increase of $d\epsilon/d\alpha$ up to an angle of attack of about
16° (fig. 15). It should be pointed out that the efficiency of the low
tail (0.074b/2) in most instances is appreciably lower than that of the
tail located 0.196 or 0.504b/2 above the wing-chord plane extended
(table II).

In the nonlinear lift range, the stability contributed by the low
tail increased over that provided in the linear lift range, whereas the
high tail exhibited a destabilizing effect in the nonlinear lift range.
Figure 15 indicates that the high tail is operating in the influence of
greatly increased $d\epsilon/d\alpha$ which is destabilizing, whereas the converse
is shown for the low tail. An explanation of stabilizing effects of
the tail entails consideration of the location of the tail relative to
the wake, which is discussed in the following section with the aid of
air-flow survey data.

The results indicate that the most favorable stabilizing effect of
the tail for the low speed range was provided with the tail located
0.074b/2 below the extended wing–chord plane.

The variation of the tail stability parameter τ (fig. 15)
indicates that the stability contributed by the tail was not changed
appreciably by the deflection of the flaps.

Air-Flow Characteristics

The results of air-flow surveys are presented as contours of
dynamic-pressure ratio, downwash angle, and sidewash angle in figures 16
and 17 for various angles of attack of both flap-on and flap-off configu-
rations. Average values of ϵ and q_t/q determined from the survey
data for 0.504, 0.196 and -0.074b/2 tail heights are presented in
table III. The average values of ϵ and q_t/q are in fair agreement
with the effective values, the largest discrepancy existing with the
low tail for configurations with flaps on. When considering the dif-
ferences between the average and effective values, it must be remembered
that the air-flow characteristics represent flow conditions at an
arbitrarily selected vertical plane normal to the tunnel center line.
In order to determine the applicability of the survey data for design
purposes, pitching moments were calculated using average values of
downwash and dynamic-pressure ratio. It was found that the agreement
with force-test data, aside from slight trim changes, was relatively
good.

An inspection of the contours of dynamic-pressure ratio for the configurations with the flaps off (fig. 16) indicates that the tail located 0.074b/2 below the extended wing-chord plane is below the wake center throughout the angle-of-attack range and that the tail heights 0.504b/2 and 0.196b/2 are above the wake center up to 23.1°. At 19° and 23.1° angle of attack, the tail height 0.196b/2 is relatively close to the center of the wake. As would be expected with the flaps on, the wake is noticeably depressed and broadened so that the low tail is enveloped up to an angle of attack of about 13°, beyond which the low tail is below the wake.

The contours of downwash angle indicate that a field of high downwash occurred above the wake center for angles of attack greater than 13°. This may be seen more readily by the example of downwash profiles presented in figure 18. From a cross plot of downwash with angle of attack (fig. 19) for several spanwise stations of the tail, it appears that all sections of the high tail are affected in the high angle-of-attack range by an adverse rate of change of downwash with angle of attack. In the case of the low tail, the variation of downwash angle with angle of attack at the tip sections is stabilizing at high angles of attack and must be highly influential in the over-all effects of the tail.

Inasmuch as the effect of the horizontal tail on the longitudinal stability depends on its location with respect to the wake, a brief study was made of the wake location of the present wing, together with similar experimental data of other wings having various plan forms. The results of this study are presented in figure 20 as the variation of dW/da (rate of change of wake center location from the wing-chord plane with angle of attack) with sweep angle for several spanwise stations of the wings considered. These results, which show a rapid increase of dW/da with sweep angle, indicate that a tail located above the wing-chord plane would be influenced by the wake more readily as the sweep angle is increased. In the determination of these slopes dW/da, the wake variations of the wings up to angles of attack where large air-flow changes occur were used. Although data at higher angles of attack were meager, the existing data for sweptback wings indicate a rapid rise of wake center location from the extended wing-chord plane with increase of angle of attack.

SUMMARY OF RESULTS

The results of a low-speed longitudinal-stability investigation of a 52° sweptback wing with various spans of leading-edge flaps, fences, a midwing fuselage, and a horizontal tail indicate that:

1. The addition of leading-edge flaps which extended over the outer 25, 35, 40, or 45 percent of the wing semispan improved the longitudinal stability characteristics of the wing through the lift range but had only a small effect on the maximum lift coefficient of the wing (1.12). From a stability consideration, the 0.40-semispan and 0.45-semispan leading-edge flaps were optimum depending on the trailing-edge-flap configuration.

2. The extended trailing-edge flaps were a considerably more effective means of increasing the lift coefficient of the wing throughout the angle-of-attack range than were split flaps.

3. The most favorable longitudinal stability characteristics and maximum-lift-coefficient results were obtained with 0.50-semispan extended trailing-edge flaps in conjunction with 0.40-semispan leading-edge flaps. With the 0.40-semispan leading-edge flaps, the wing was stable and had a maximum lift coefficient of 1.19. The addition of the 0.50-semispan extended trailing-edge flaps provided a maximum lift coefficient of 1.36 and the stability was maintained throughout the lift range.

4. The fuselage decreased the stability near maximum lift coefficient of the configuration with 0.40-semispan leading-edge flaps. The destabilizing effect of the fuselage was not obtained for configurations with fences or with 0.25-semispan leading-edge flaps.

5. In the high angle-of-attack range the tail located below the wing-chord plane extended is below the wake and in a region where the rate of change of downwash with angle of attack is stabilizing. Tail positions above the wing-chord plane extended are either in or above the wake and are adversely affected by the rate of change of downwash with angle of attack. In general, stability throughout the angle-of-attack range was obtained for configurations with the tail located below the wing-chord plane extended; whereas, for most configurations with the tail located above the wing-chord plane extended, instability, or a very small degree of stability, was obtained in the high angle-of-attack range.
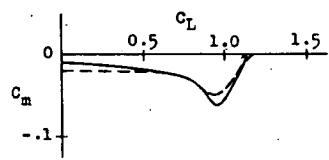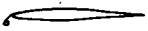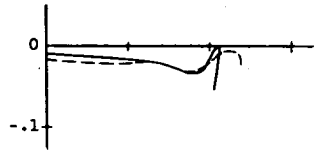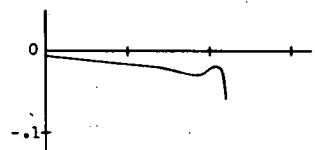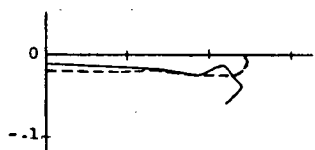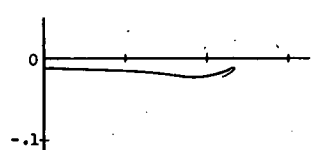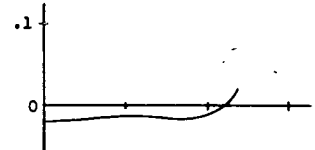
Langley Aeronautical Laboratory
    National Advisory Committee for Aeronautics
        Langley Field, Va.

REFERENCES

1. Graham, Robert R., and Conner, D. William: Investigation of High-
   Lift and Stall-Control Devices on an NACA 64-Series 42° Swept-
   back Wing with and without Fuselage. NACA RM L7G09, 1947.

2. Foster, Gerald V., and Griner, Roland F.: Low-Speed Longitudinal
   Characteristics of a Circular-Arc 52° Sweptback Wing of Aspect
   Ratio 2.84 with and without Leading-Edge and Trailing-Edge Flaps
   at Reynolds Numbers from 1.6×10^6 to 9.7×10^6. NACA RM L50F16a,
   1950.

3. Fitzpatrick, James E., and Foster, Gerald V.: Static Longitudinal
   Aerodynamic Characteristics of a 52° Sweptback Wing of Aspect
   Ratio 2.88 at Reynolds Numbers from 2,000,000 to 11,000,000.
   NACA RM L8H25, 1948.

4. Foster, Gerald V., and Fitzpatrick, James E.: Longitudinal-
   Stability Investigation of High-Lift and Stall-Control Devices
   on a 52° Sweptback Wing with and without Fuselage and Horizontal
   Tail at a Reynolds Number of 6.8×10^6. NACA RM L8I08, 1948.

5. Salmi, Reino J.: Effects of Leading-Edge Devices and Trailing-Edge
   Flaps on Longitudinal Characteristics of Two 47.7° Sweptback
   Wings of Aspect Ratios 5.1 and 6.0 at a Reynolds Number of
   6.0×10^6. NACA RM L50F20, 1950.

6. Furlong, G. Chester, and Bollech, Thomas V.: Downwash, Sidewash,
   and Wake Surveys behind a 42° Sweptback Wing at a Reynolds Number
   of 6.8×10^6 with and without a Simulated Ground. NACA RM L8G22,
   1948.

7. Eisenstadt, Bertram J.: Boundary-Induced Upwash for Yawed and
   Swept-Back Wings in Closed Circular Wind Tunnels. NACA TN 1265,
   1947.

8. Spooner, Stanley H., and Martina, Albert P.: Longitudinal Stability
   Characteristics of a 42° Sweptback Wing and Tail Combination at
   a Reynolds Number of 6.8×10^6. NACA RM L8E12, 1948.

9. Neely, Robert H., and Koven, William: Low-Speed Characteristics in
   Pitch of a 42° Sweptback Wing with Aspect Ratio 3.9 and Circular-
   Arc Airfoil Sections. NACA RM L7E23, 1947.

10. Hoggard, H. Page, Jr., and Hagerman, John R.: Downwash and Wake
    behind Untapered Wings of Various Aspect Ratios and Angles of
    Sweep. NACA TN 1703, 1948.

11. Salmi, Reino J.: Horizontal-Tail Effectiveness and Downwash
     Surveys for Two 47.7° Sweptback Wing-Fuselage Combinations with
     Aspect Ratios of 5.1 and 6.0 at a Reynolds Number of 6.0×10^6.
     NACA RM L50K06, 1950.

TABLE I.- SUMMARY OF AERODYNAMIC CHARACTERISTICS OF A 52° SWEPTBACK WING WITH
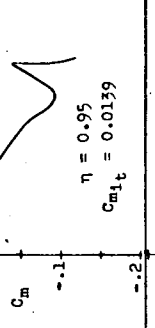AND WITHOUT SEVERAL COMBINATIONS OF LEADING- AND TRAILING-EDGE FLAPS.

Configuration	Flap span (b/2)	C_{Lmax}	$^a C_{Lmax}$	D/L at 0.85 C_{Lmax}	C_m characteristics (a)	Fig.
	off	1.12	25.5	0.190		4
	0.250	1.07	27.4	.176		4
	.350	1.10	30.0	.188		4
	.400	1.19	29.2	.275		8
	.450	1.13	28.6	.198		4
	.575	1.17	^{b} 28.2	.195		4

^{a}Dashed line indicates configuration with midwing fuselage.
^{b}Maximum angle of attack tested.

TABLE I.- SUMMARY OF AERODYNAMIC CHARACTERISTICS OF A 52° SWEPTBACK WING - CONCLUDED.
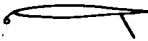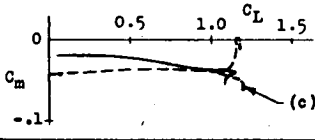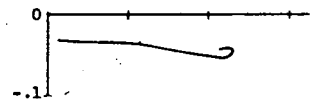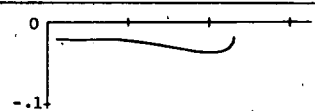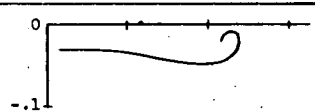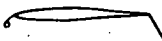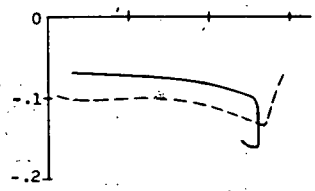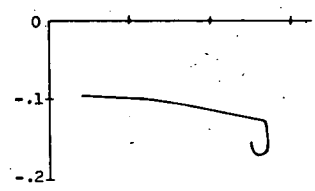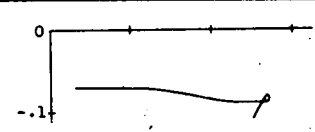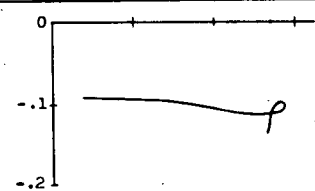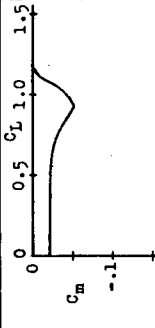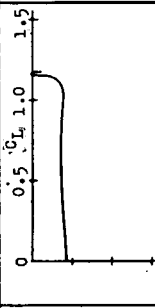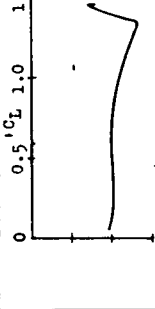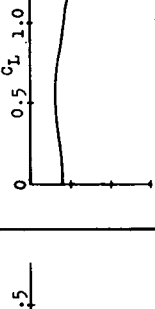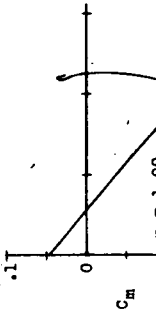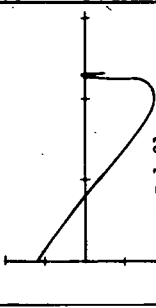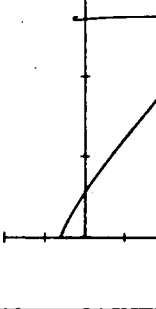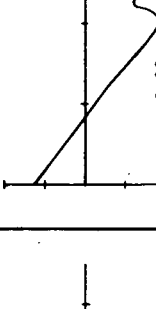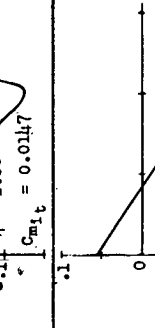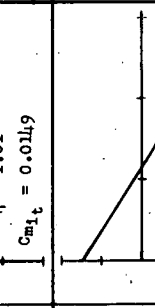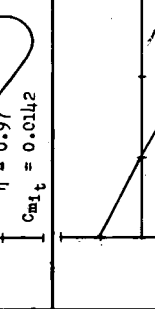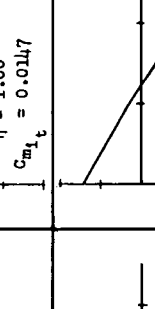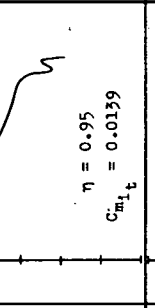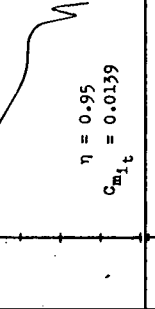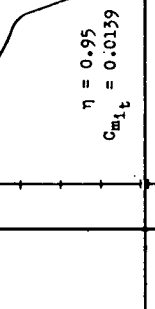
Configuration	Flap span (b/2)	C_{Lmax}	$\alpha_{C_{Lmax}}$	D/L at 0.85 C_{Lmax}	C_m characteristics (a)	Fig.
	L.E. 0.40 T.E. 0.40	1.14	24.7	.179		8
	L.E. 0.40 T.E. 0.50	1.17	23.0	.181		8
	L.E. 0.45 T.E. 0.40	1.15	23.0	.176		6
	L.E. 0.45 T.E. 0.50	1.19	22.8	.183		6
	L.E. 0.40 T.E. 0.40	1.31	23.5	.182		9
	L.E. 0.40 T.E. 0.50	1.36	24.0	.202		9
	L.E. 0.45 T.E. 0.40	1.35	24.0	.189		7
	L.E. 0.45 T.E. 0.50	1.44	25.5	.207		7

[a] Dashed line indicates configuration with midwing fuselage.

[c] Mid-wing fuselage configuration with fences located at 0.65b/2 from plane of symmetry.

Table II.- SUMMARY OF PITCHING-MOMENT CHARACTERISTICS OF A 52° SWEPTBACK WING WITH
LEADING- AND TRAILING-EDGE FLAPS, MIDWING FUSELAGE, AND A HORIZONTAL TAIL.

Tail position ($2 z/b$)	Wing configuration			
	Flaps off	0.40b/2 leading-edge flaps .40b/2 split flaps	0.40b/2 leading-edge flaps .40b/2 extended trailing-edge flaps	0.40b/2 leading-edge flaps .40b/2 split flaps (a)
Off				
0.504	$\eta = 1.00$ $C_{m_{i_t}} = 0.0147$	$\eta = 1.01$ $C_{m_{i_t}} = 0.0149$	$\eta = 0.97$ $C_{m_{i_t}} = 0.0142$	$\eta = 1.00$ $C_{m_{i_t}} = 0.0147$
0.196	$\eta = 0.95$ $C_{m_{i_t}} = 0.0139$	$\eta = 0.95$ $C_{m_{i_t}} = 0.0139$	$\eta = 0.95$ $C_{m_{i_t}} = 0.0139$	$\eta = 0.95$ $C_{m_{i_t}} = 0.0139$
-0.074	$\eta = 0.95$ $C_{m_{i_t}} = 0.0139$	$\eta = 0.87$ $C_{m_{i_t}} = 0.0128$	$\eta = 0.83$ $C_{m_{i_t}} = 0.0122$	$\eta = 0.80$ $C_{m_{i_t}} = 0.0117$

(a) Configuration includes fences located 0.65b/2.

TABLE III

EFFECTIVE AND AVERAGE VALUES OF DYNAMIC-PRESSURE RATIO AND DOWNWASH ANGLE

AT THE TAIL OF A 52° SWEPTBACK WING-FUSELAGE COMBINATION

Tail height b/2		α 3.3° Flaps Off	3.3° Flaps On	8.1° Flaps Off	8.1° Flaps On	13.0° Flaps Off	13.0° Flaps On	16.3° Flaps Off	16.3° Flaps On	19.0° Flaps Off	19.0° Flaps On	23.1° Flaps Off	23.1° Flaps On
0.504	$(q_t/q)_{av}$	—	—	0.98	0.98	0.98	0.99	0.98	1.00	1.02	1.00	1.02	0.91
	$(q_t/q)_e$	1.00	1.00	1.00	1.00	1.00	1.00	1.00	1.06	1.00	1.07	1.00	0.87
	ϵ_{av}	—	—	4.4°	5.5°	6.6°	7.7°	8.2°	9.8°	11.2°	12.5°	18.3°	21.4°
	ϵ_e	3.7°	4.5°	5.4°	6.3°	7.3°	8.3°	8.6°	10.7°	11.4°	13.7°	19.0°	20.1°
0.196	$(q_t/q)_{av}$	0.95	0.97	0.94	0.96	0.93	0.94	0.88	0.94	0.84	0.88	0.86	0.76
	$(q_t/q)_e$	1.00	1.00	1.00	1.00	1.00	1.00	0.98	1.00	0.97	0.98	0.96	0.83
	ϵ_{av}	3.7°	5.3°	6.6°	7.8°	9.5°	10.7°	11.4°	13.1°	13.1°	16.5°	17.6°	16.1°
	ϵ_e	4.7°	6.3°	7.0°	8.3°	9.6°	11.0°	11.4°	13.5°	12.8°	15.9°	17.0°	16.7°
-0.074	$(q_t/q)_{av}$	0.94	0.82	0.94	0.88	0.94	0.84	0.95	0.79	0.95	0.84	0.98	0.96
	$(q_t/q)_e$	1.00	1.00	1.00	1.00	1.00	1.00	1.00	1.00	1.00	1.00	1.00	1.00
	ϵ_{av}	-0.2°	1.3°	2.7°	4.1°	5.6°	5.9°	6.7°	7.0°	7.0°	6.7°	7.8°	6.5°
	ϵ_e	-0.4°	1.4°	2.1°	3.5°	4.4°	5.5°	5.9°	6.6°	6.4°	7.0°	8.1°	6.7°

Note: Flaps on -- 0.40b/2 leading-edge flaps
and 0.40b/2 split flaps.
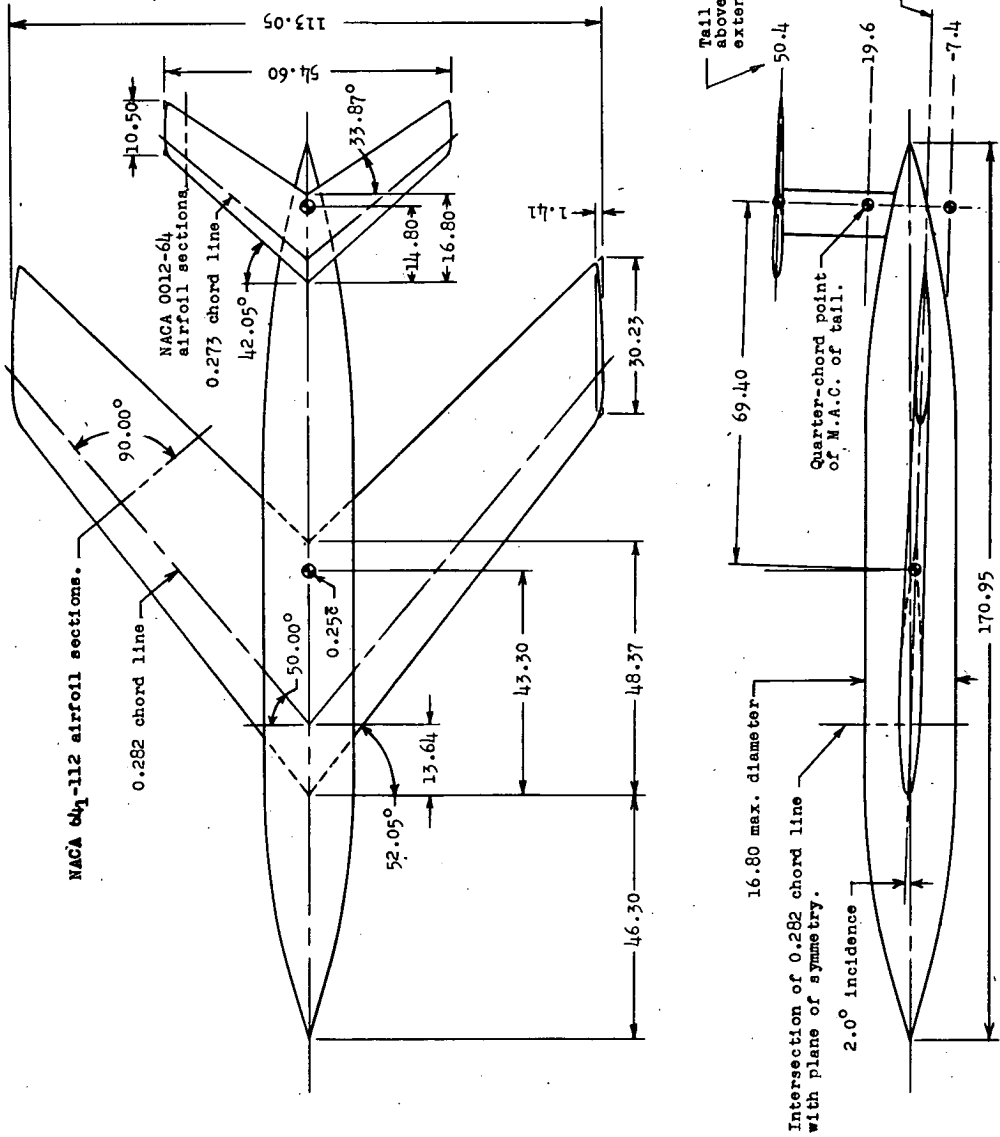
Figure 1.- Geometry of 52° sweptback wing with fuselage and horizontal tail. Wing: aspect ratio, 2.88; taper ratio, 0.625; area, 4429 sq in.; $\bar{c}$ = 39.97. All dimensions are in inches.
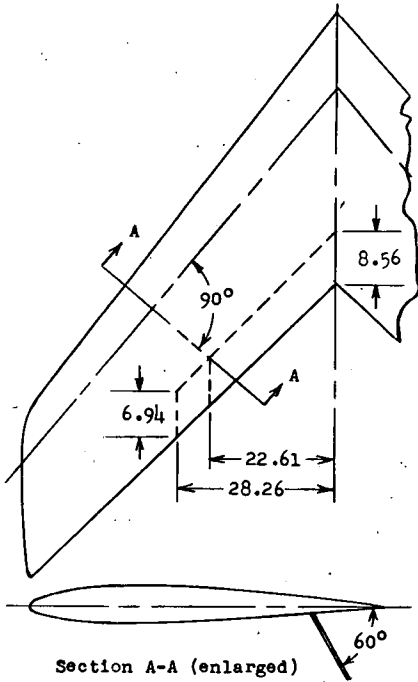
Section A-A (enlarged)

(a) Split flap.
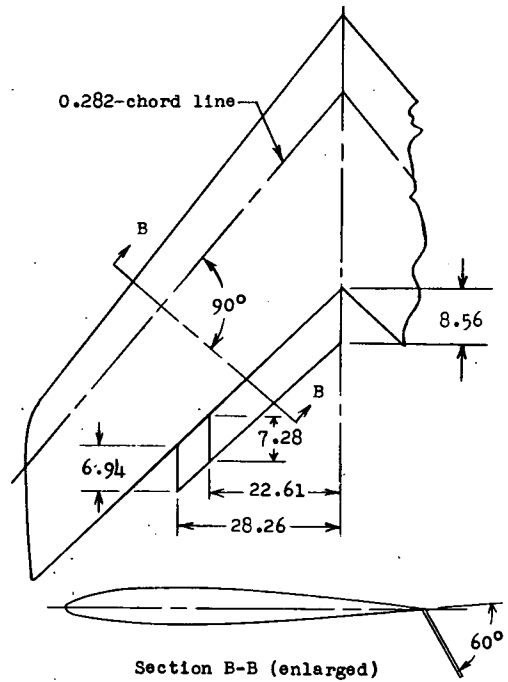
Section B-B (enlarged)

(b) Extended trailing-edge flap.
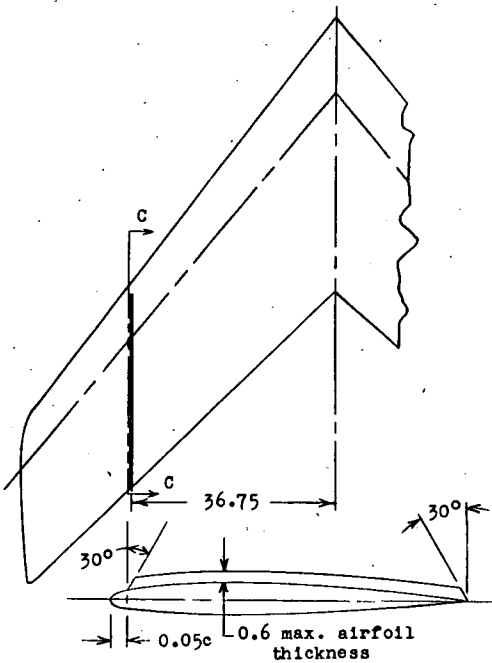
Section C-C (enlarged)

(c) Fence.

L. E. flap	d (b/2)
A	0.250
AB	.350
ABC	.400
ABCD	.450
ABCDE	.575
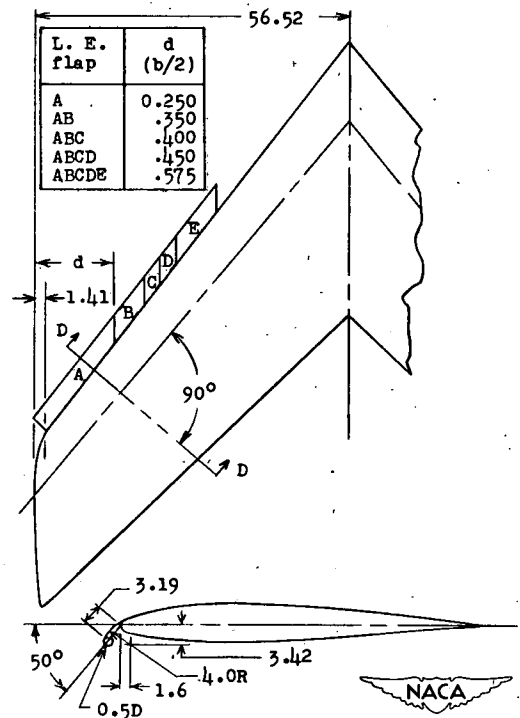
Section D-D (enlarged)

(d) Leading-edge flap.

Figure 2.- Details of split flaps, extended trailing-edge flaps, fences, and leading-edge flaps on a 52° sweptback wing. All dimensions are in inches unless otherwise noted.
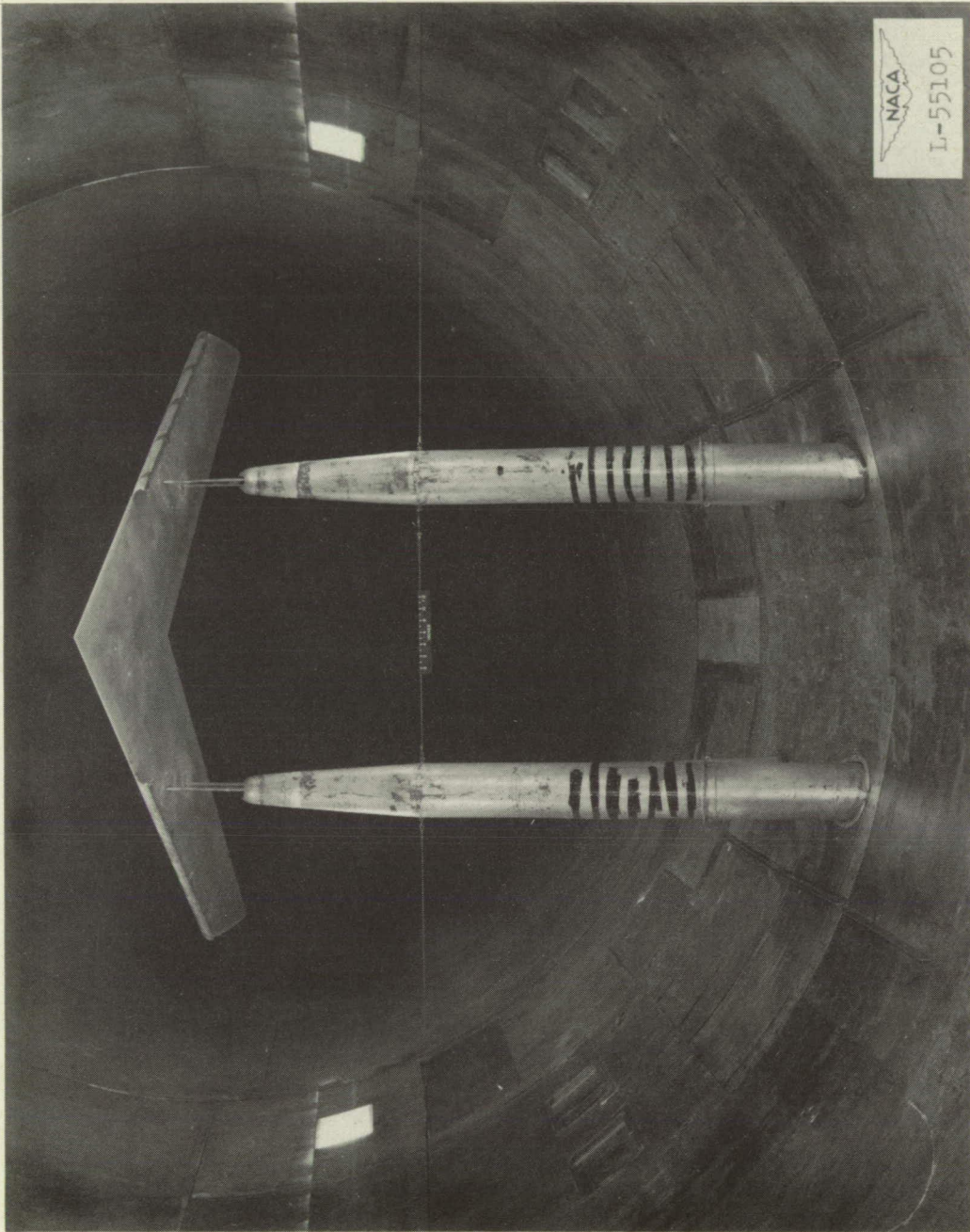
Figure 3.- The 52° sweptback wing mounted for testing in the Langley 19-foot pressure tunnel.
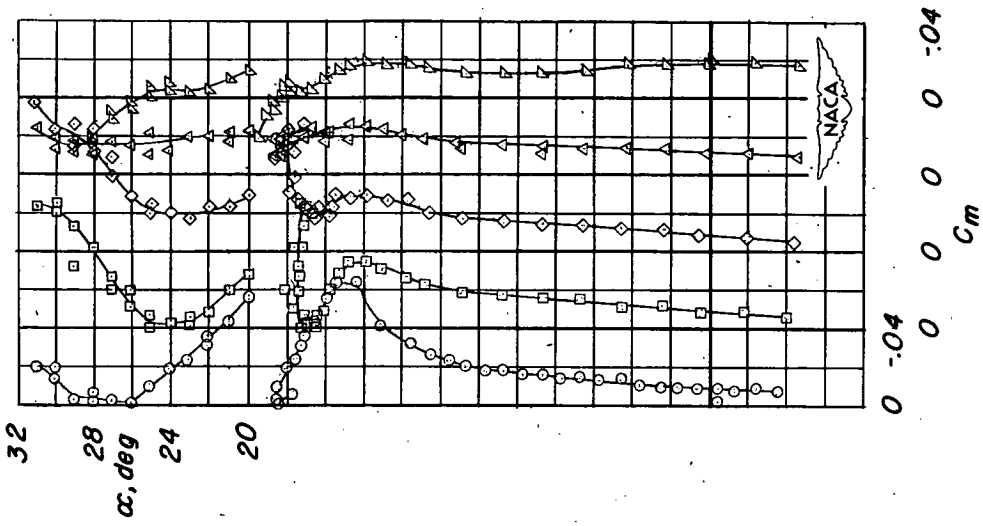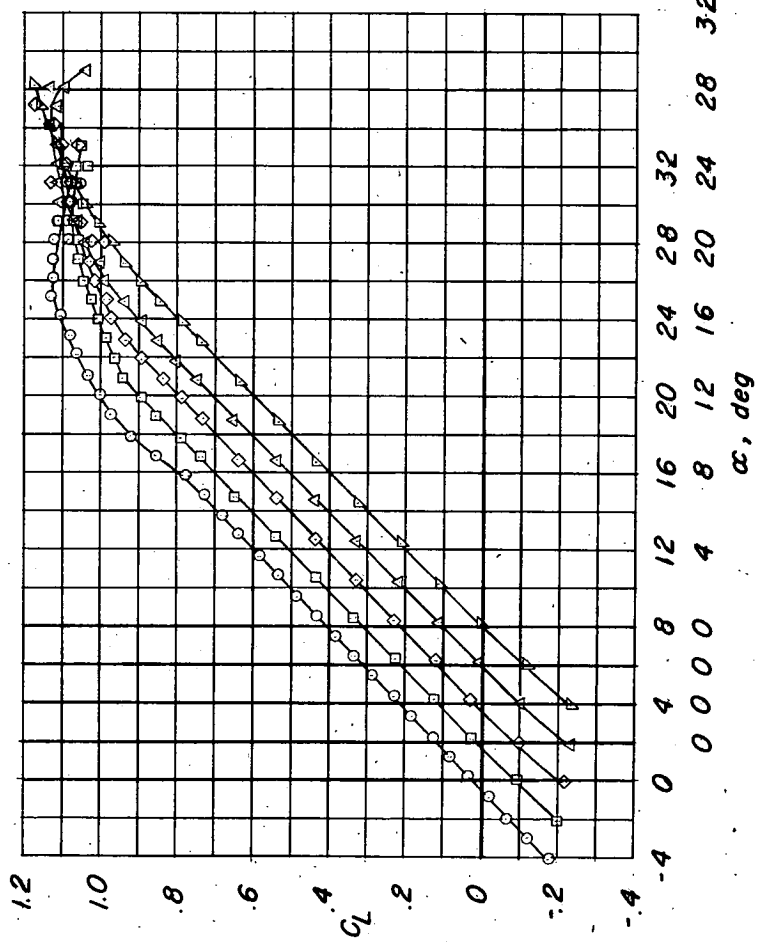
(a) Variation of C_m and α with C_L.

Figure 4.- Aerodynamic characteristics of a 52° sweptback wing with extensible leading-edge flaps of various spans.
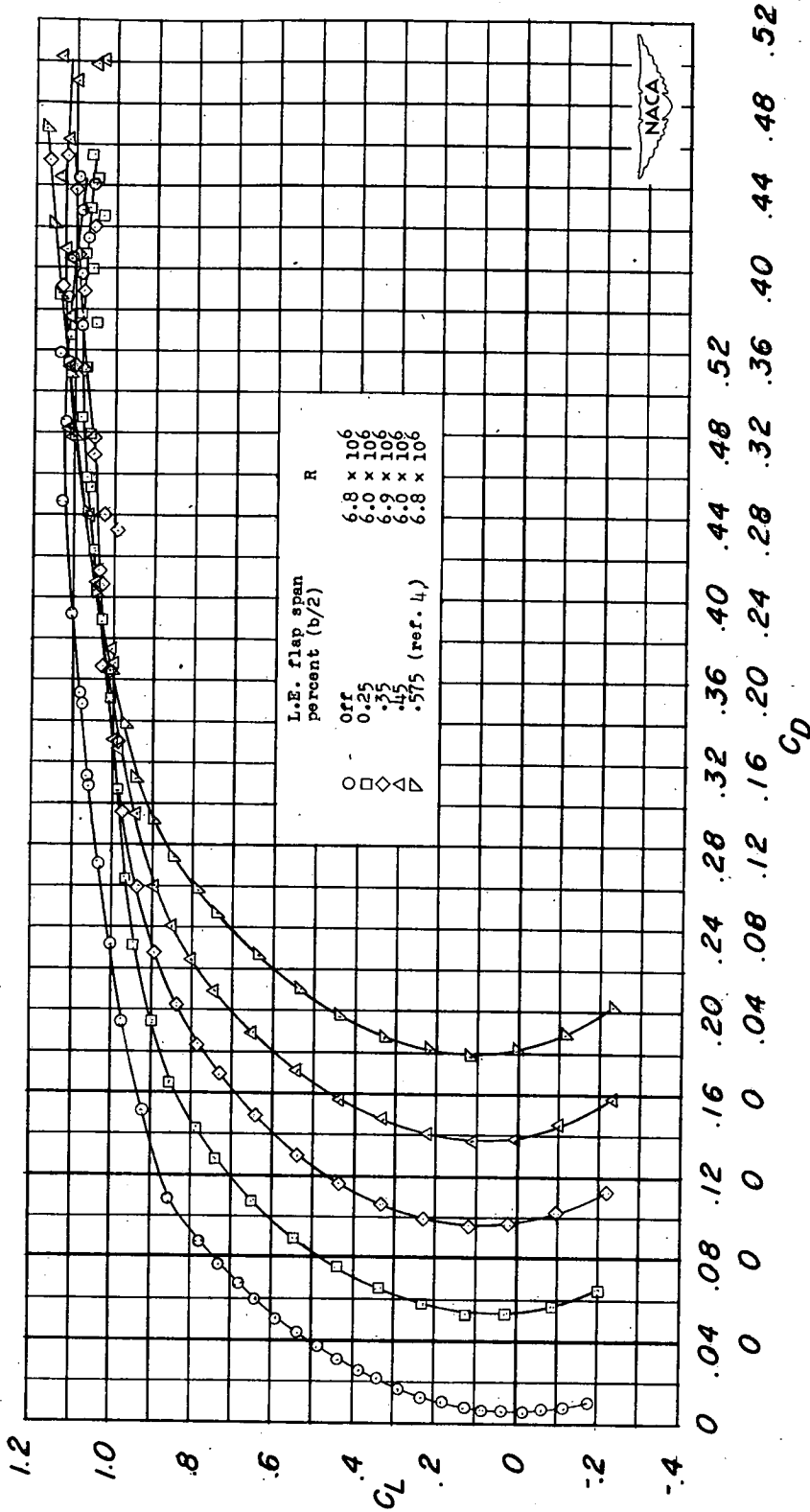
(b) Variation of C_D with C_L.

Figure 4.- Concluded.
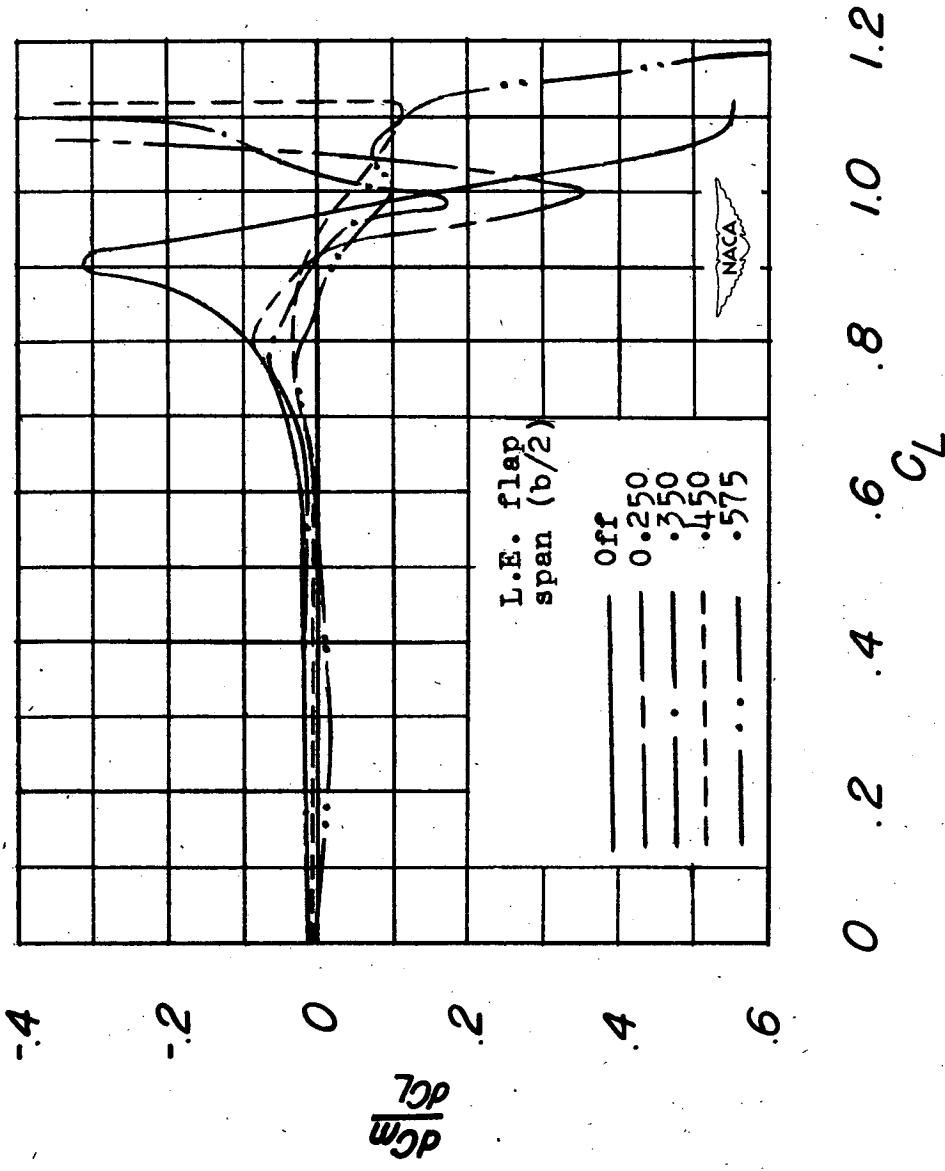
Figure 5.- Variation of dC_m/dC_L with lift coefficient for a 52^0 sweptback wing with various spans of extensible leading-edge flaps.
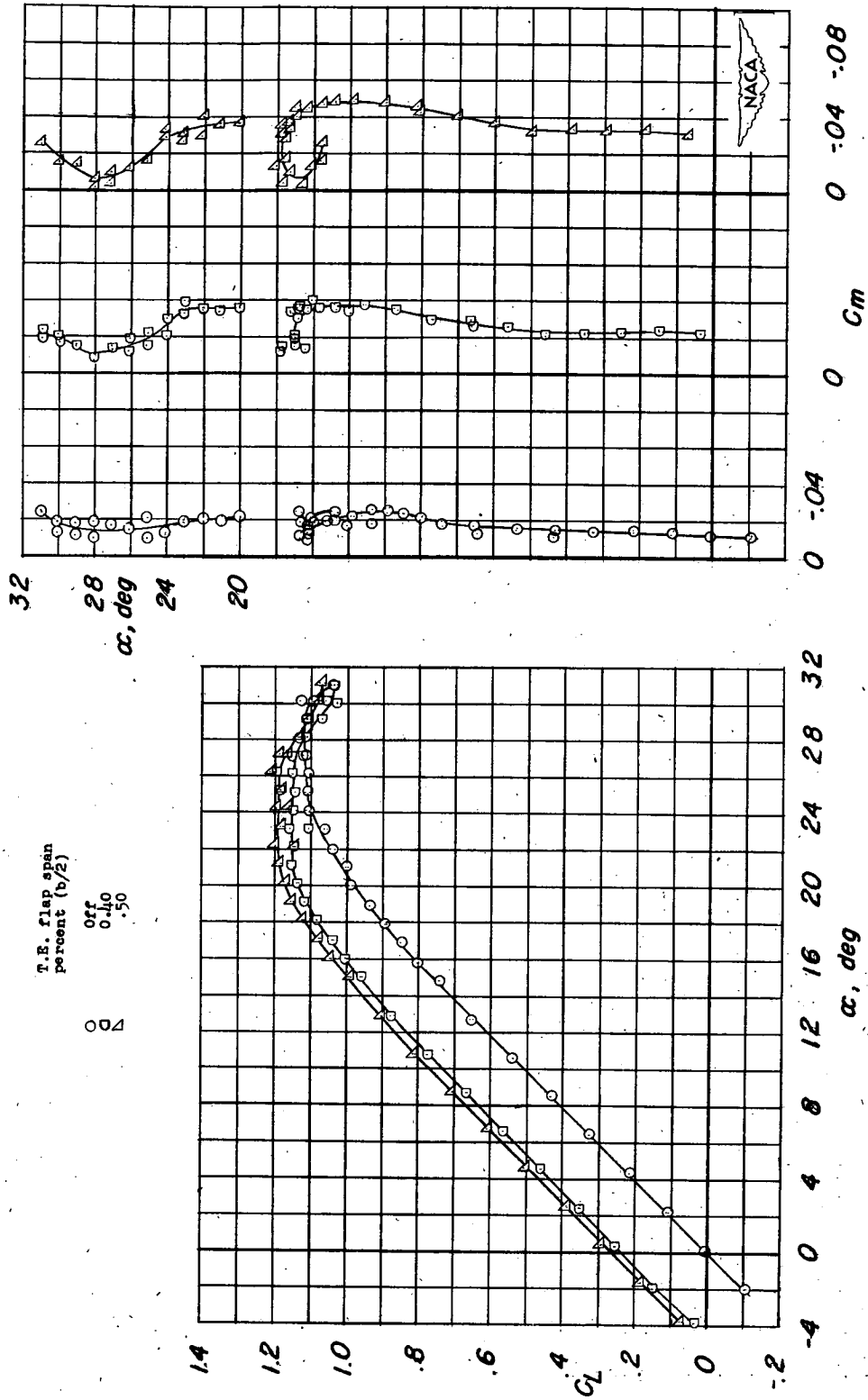
(a) Variation of C_m and α with C_L.

Figure 6.- The effect of several spans of split flaps on the aerodynamic characteristics of a 52° sweptback wing with 0.45b/2 extensible leading-edge flaps. R = 6.0 × 10⁶.
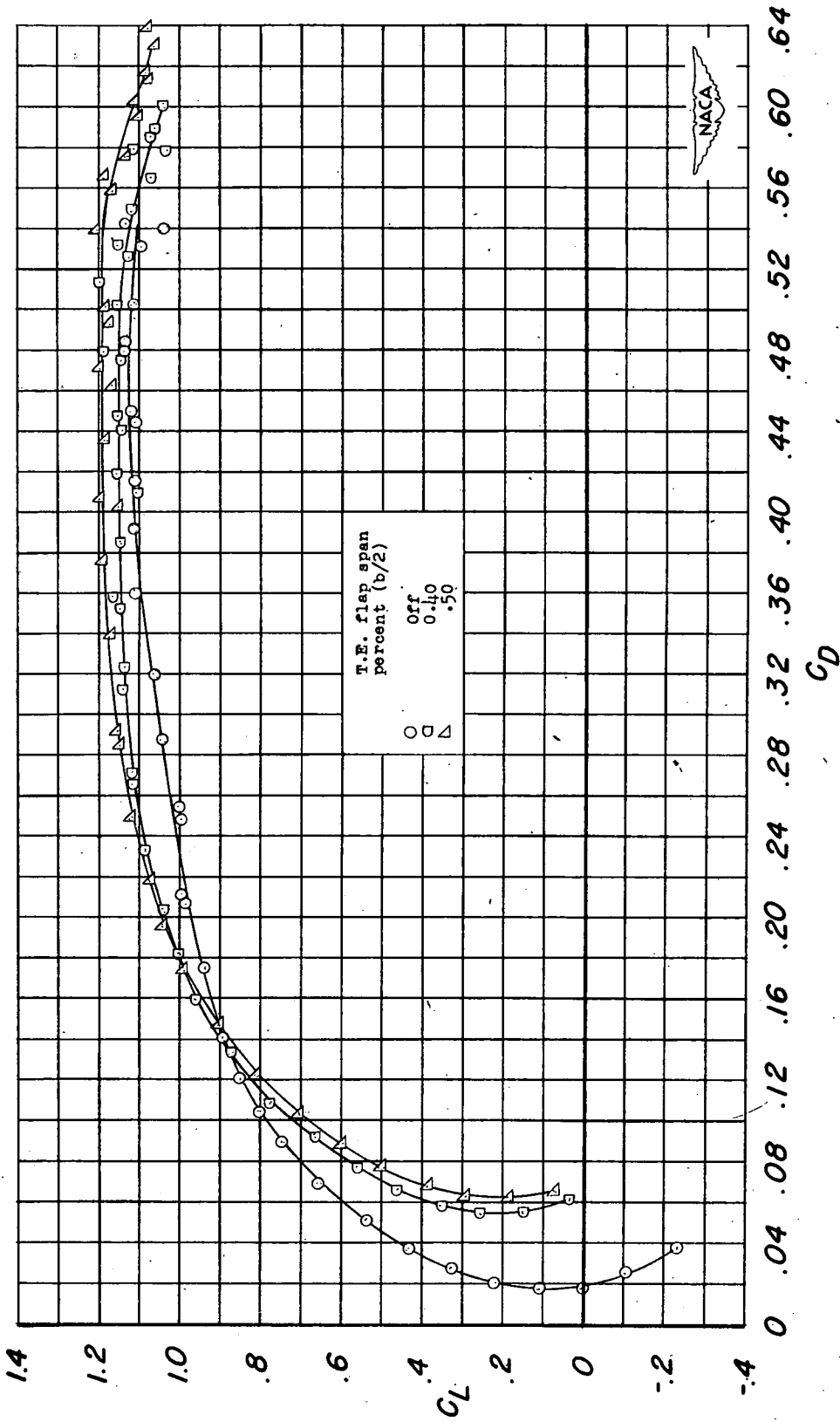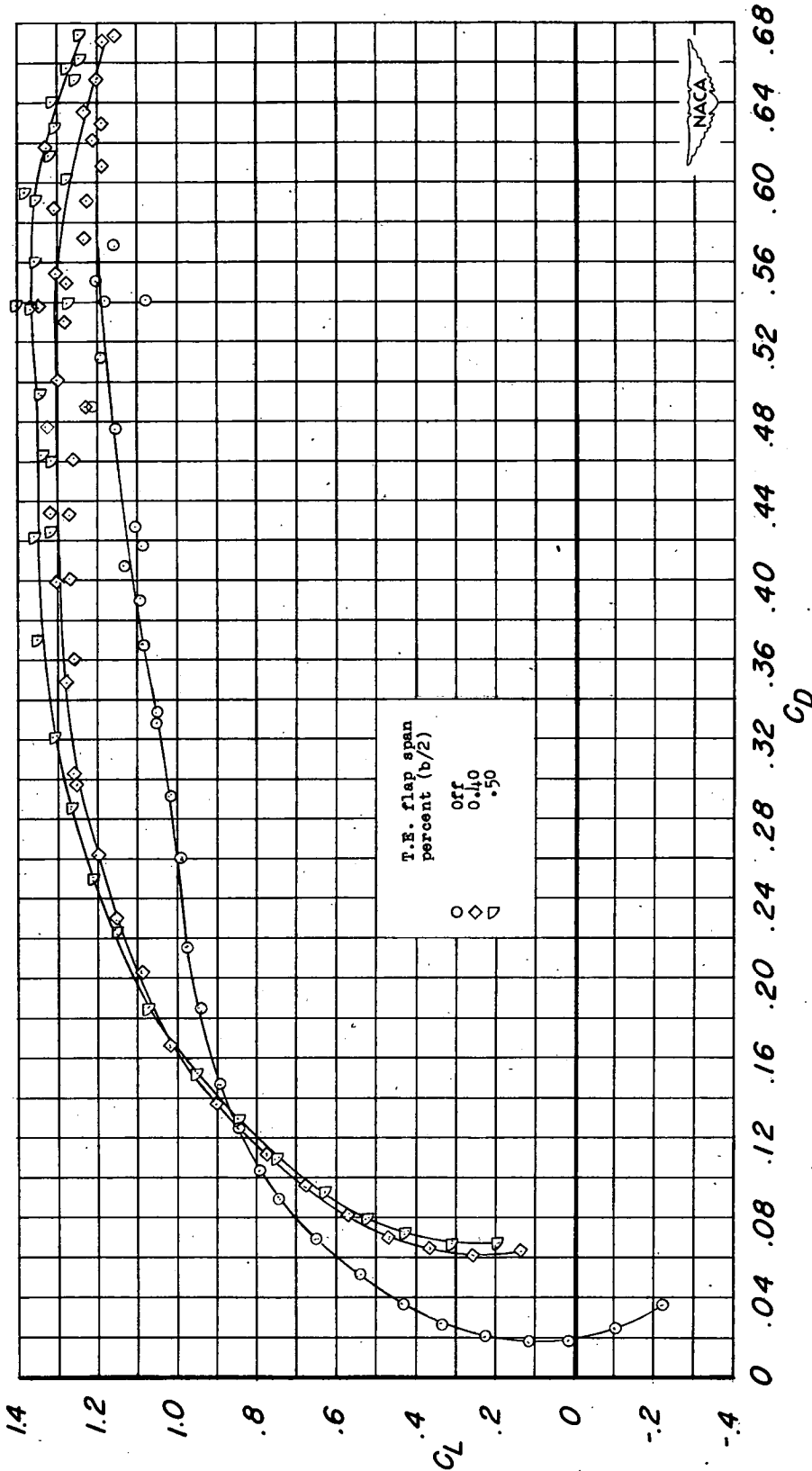
(b) Variation of C_D with C_L.

Figure 6.- Concluded.
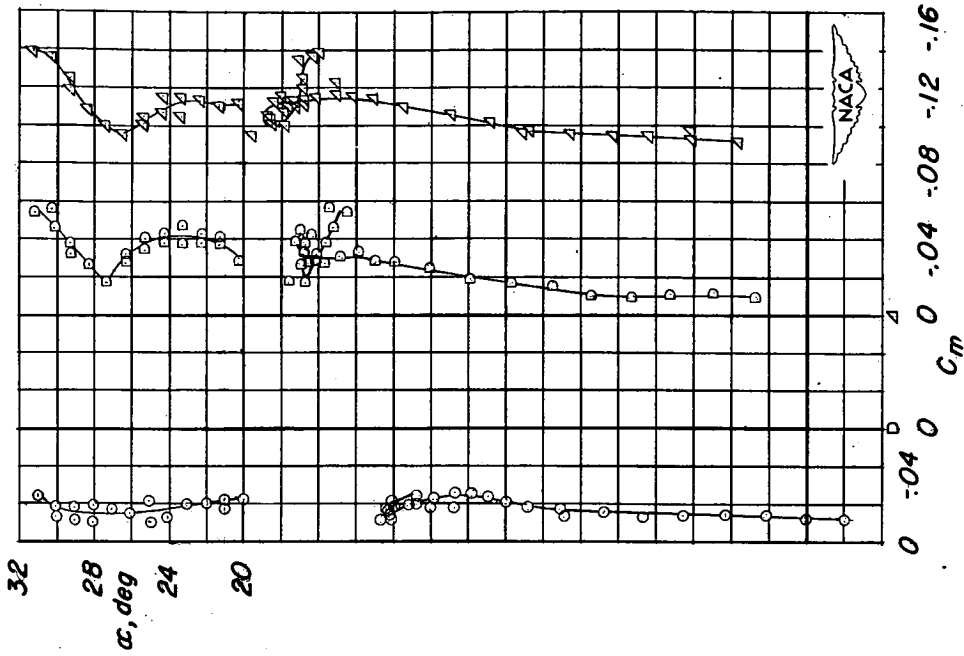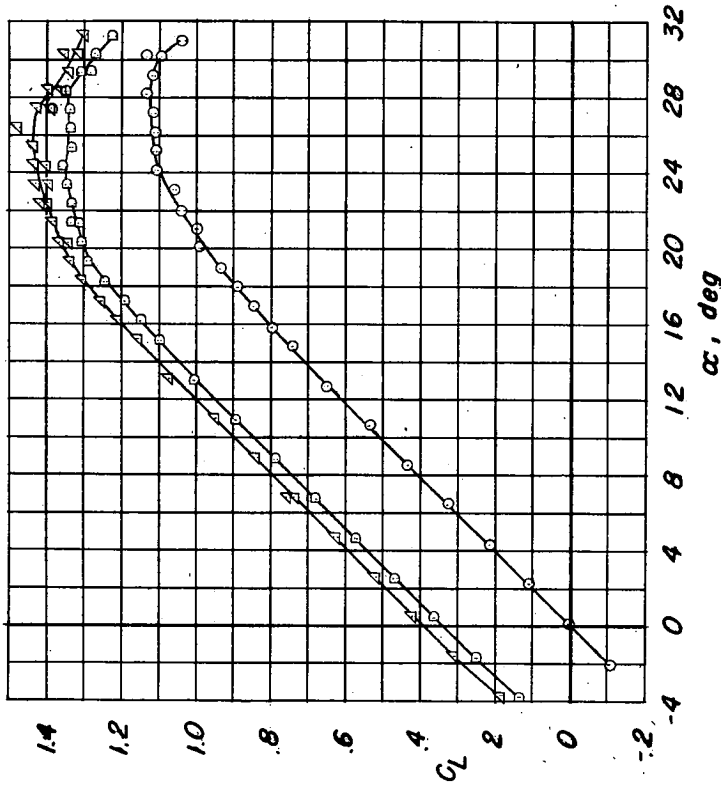
(a) Variation of C_m and α with C_L.

Figure 7.- The effect of several spans of extended trailing-edge flaps on the aerodynamic characteristics of a 52° sweptback wing with 0.45b/2 extensible leading-edge flaps. $R = 6.0 \times 10^6$.
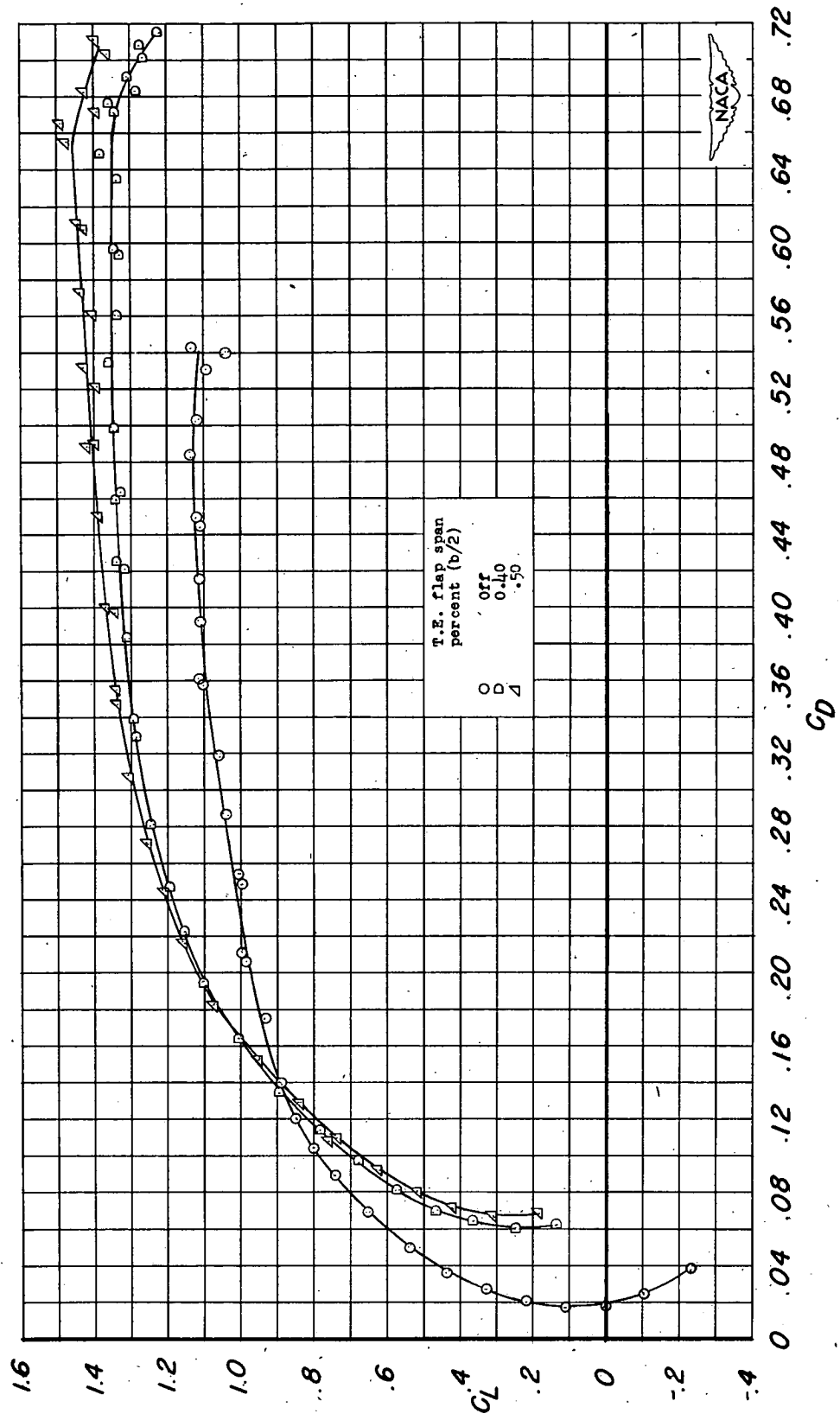
(b) Variation of C_D with C_L.

Figure 7.- Concluded.
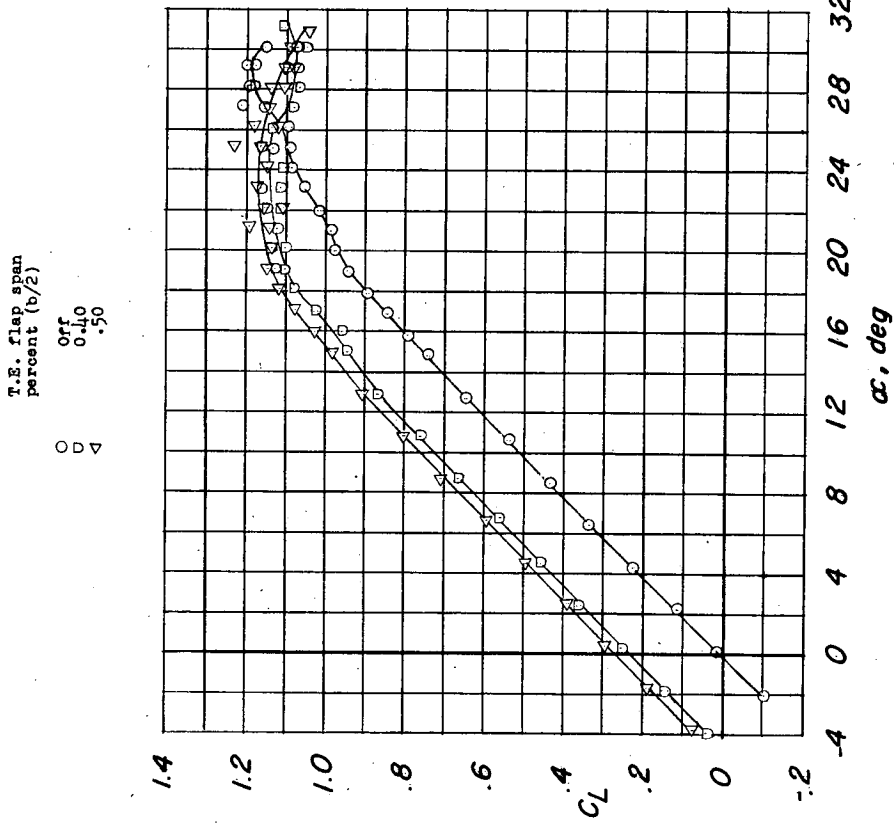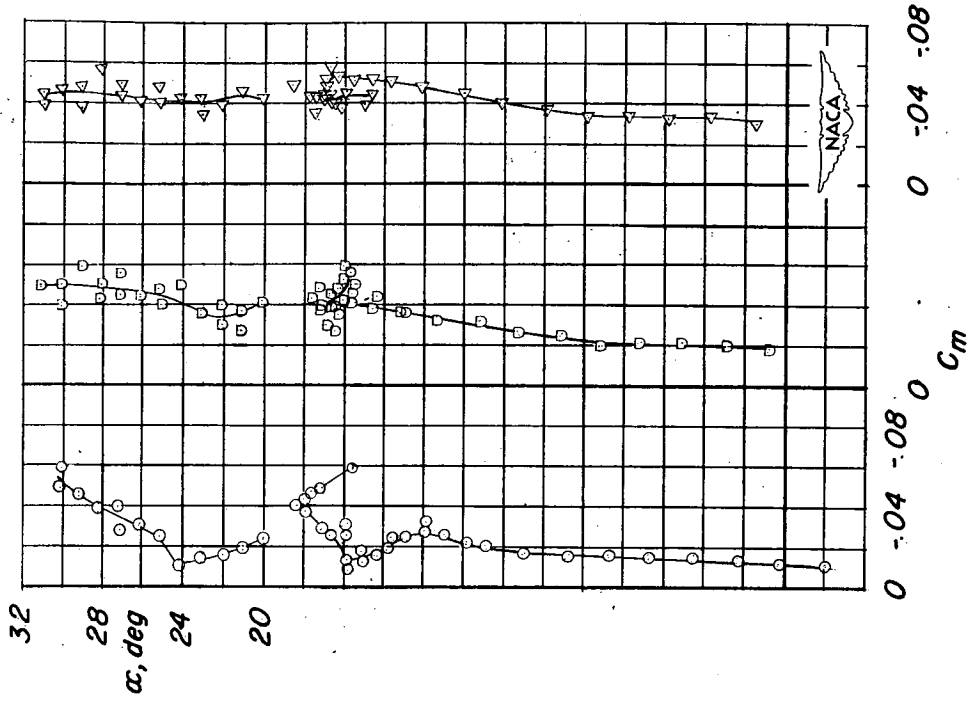
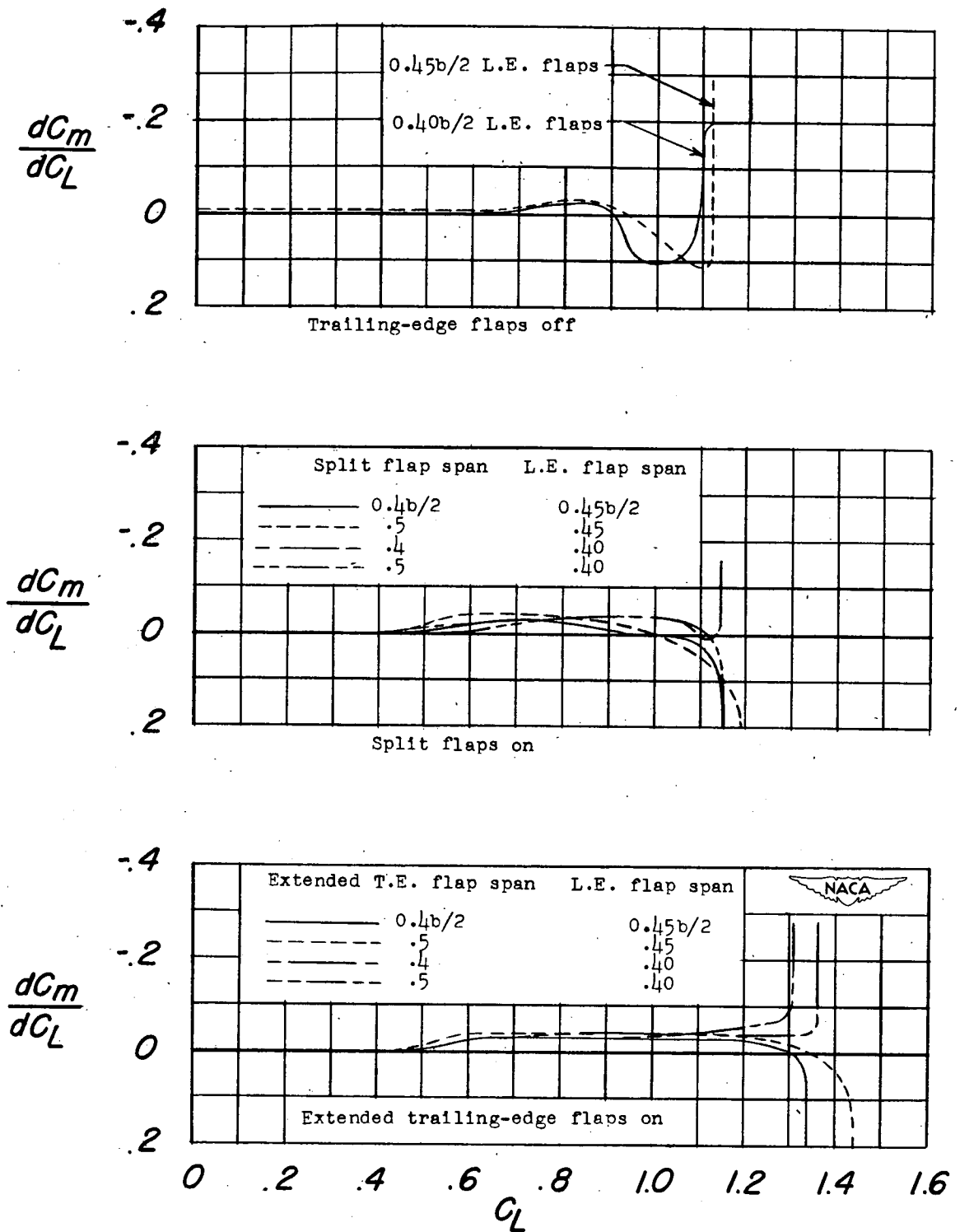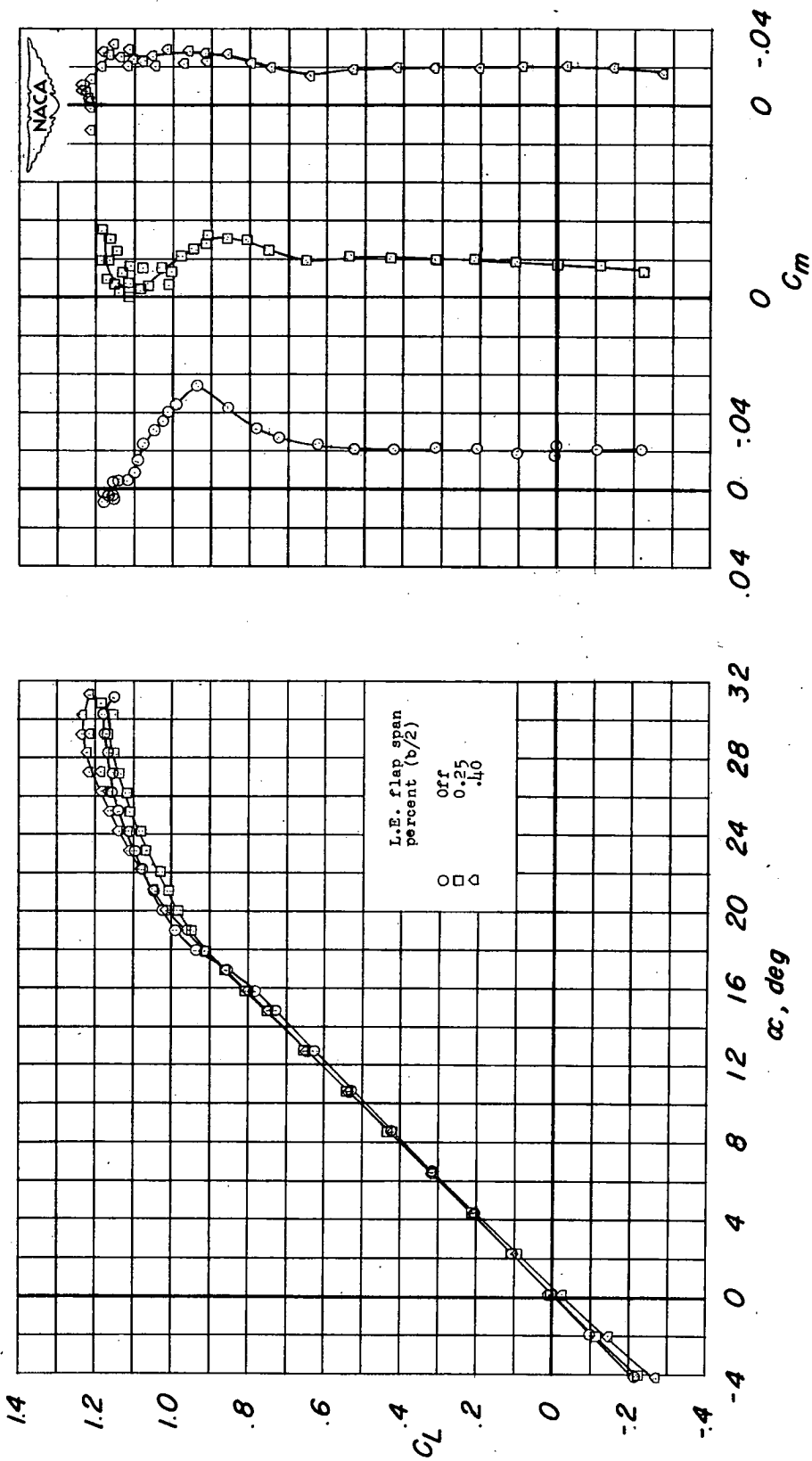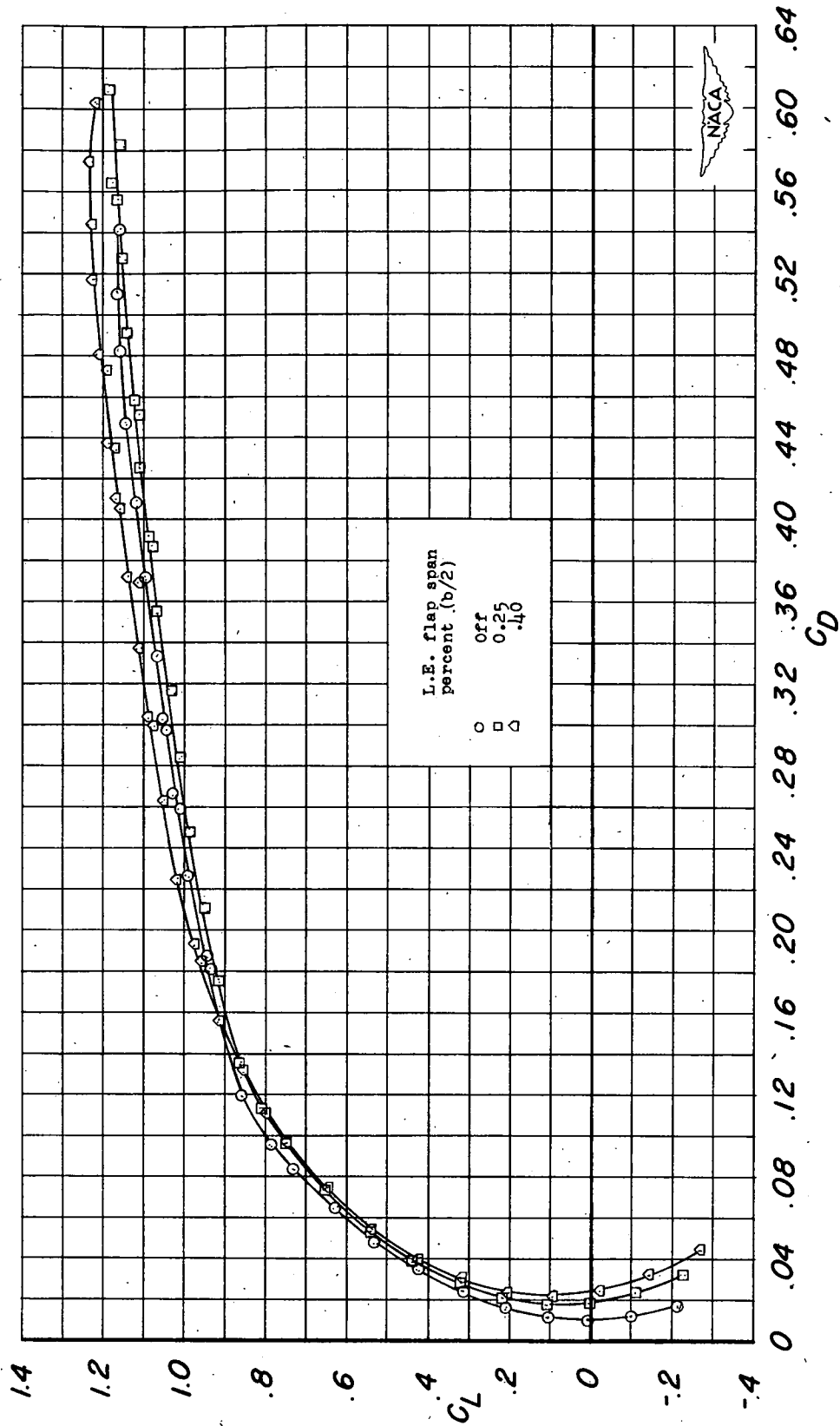(a) Variation of C_m and α with C_L.

Figure 8.- The effect of several spans of split flaps on the aerodynamic characteristics of a 52° sweptback wing with 0.40b/2 extensible leading-edge flaps. R = 6.0 × 10⁶.
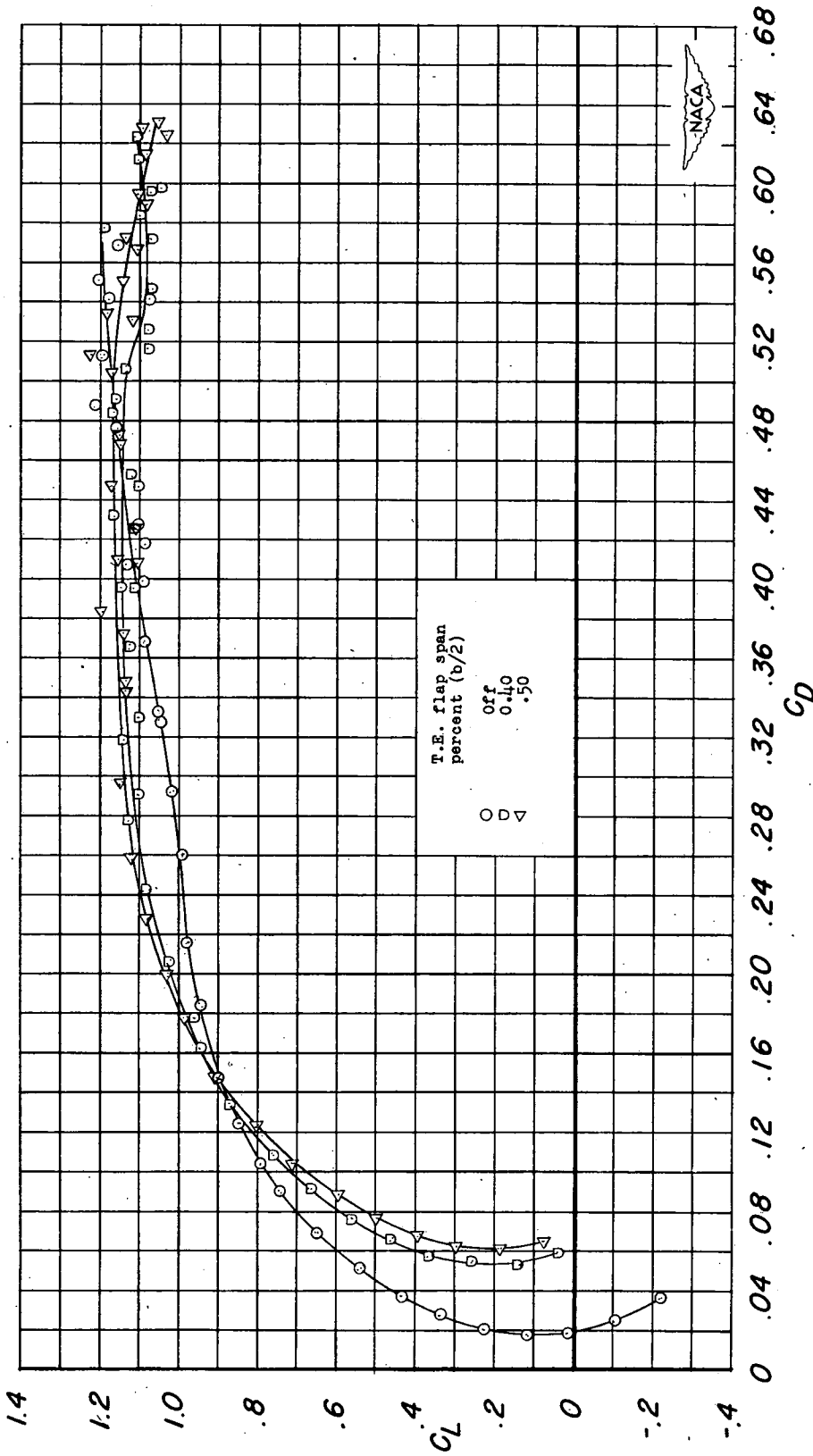
(b) Variation of C_D with C_L.

Figure 8.- Concluded.
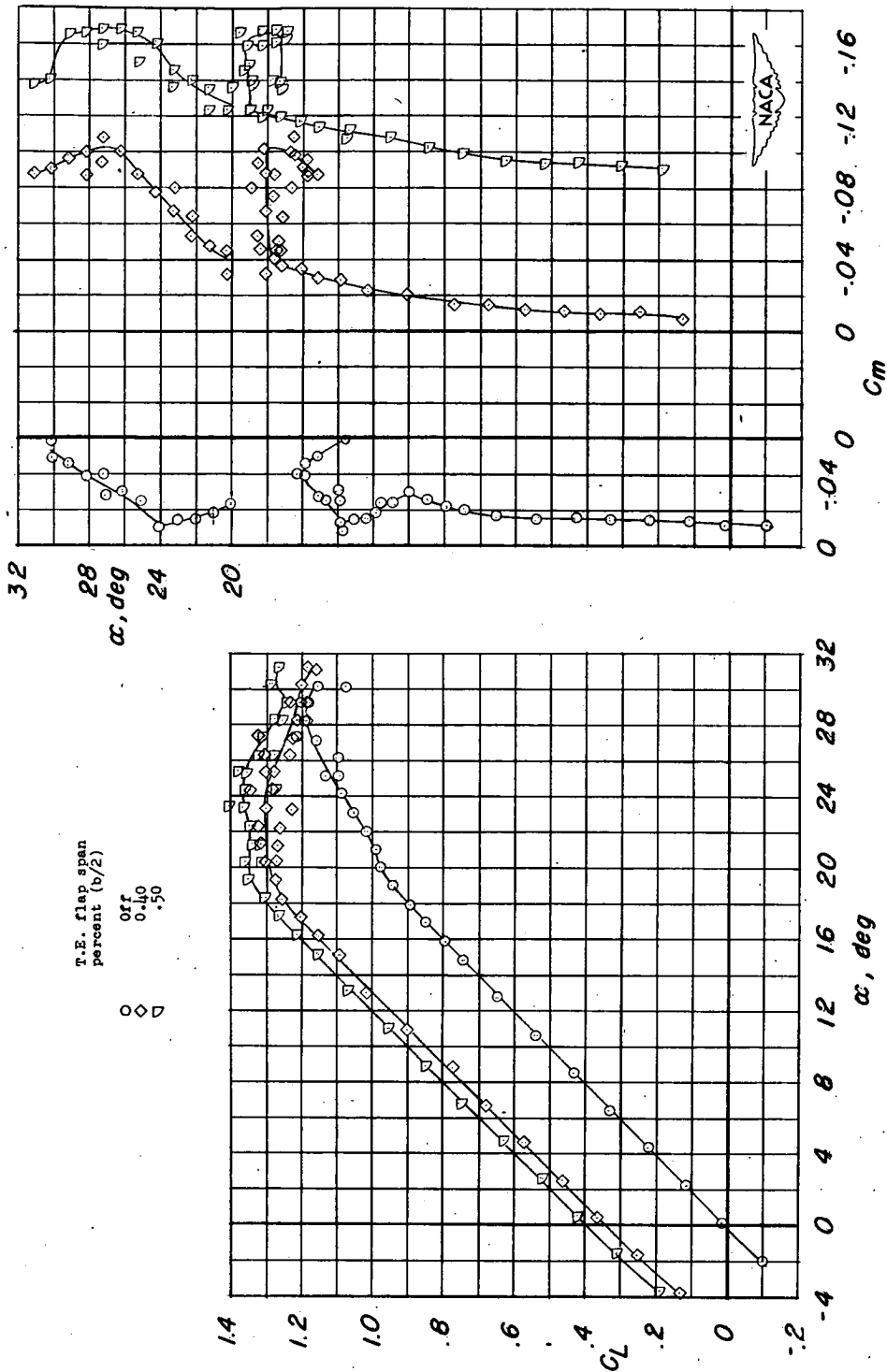
(a) Variation of C_m and α with C_L.

Figure 9.- The effect of several spans of extended trailing-edge flaps on the aerodynamic characteristics of a 52° sweptback wing with 0.40b/2 extensible leading-edge flaps. R = 6.0 × 10⁶.

(b) Variation of C_D with C_L.

Figure 9.- Concluded.

Figure 10.- Effect of 0.40b/2 and 0.45b/2 leading-edge flaps on the
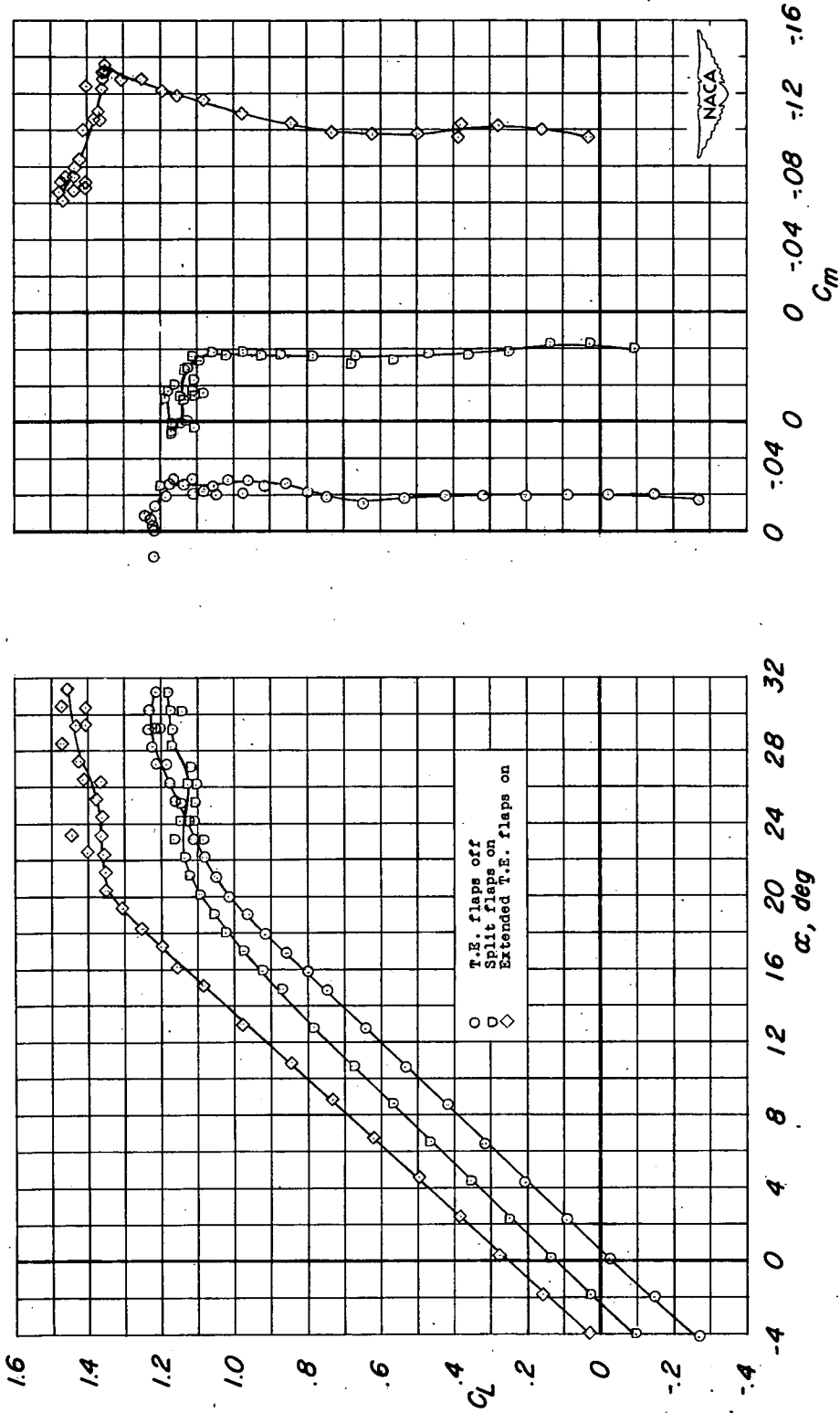variation of dC_m/dC_L.

(a) Variation of C_m and α with C_L.

Figure 11.- The effect of several spans of extensible leading-edge flaps on
the aerodynamic characteristics of a 52° sweptback wing with a fuselage;
midwing combination. R = 6.0 × 10⁶.

(b) Variation of C_D with C_L.

Figure 11.- Concluded.
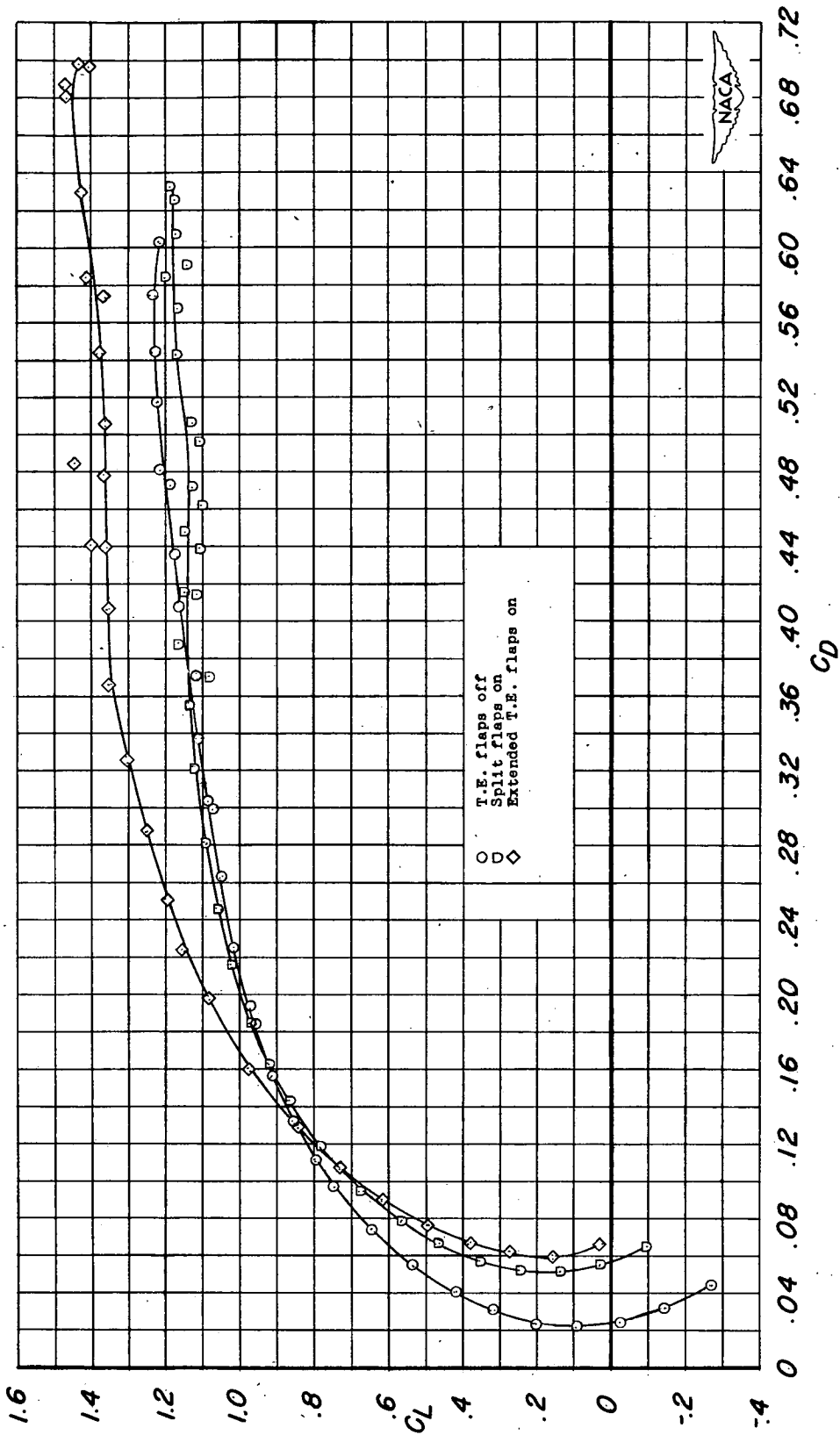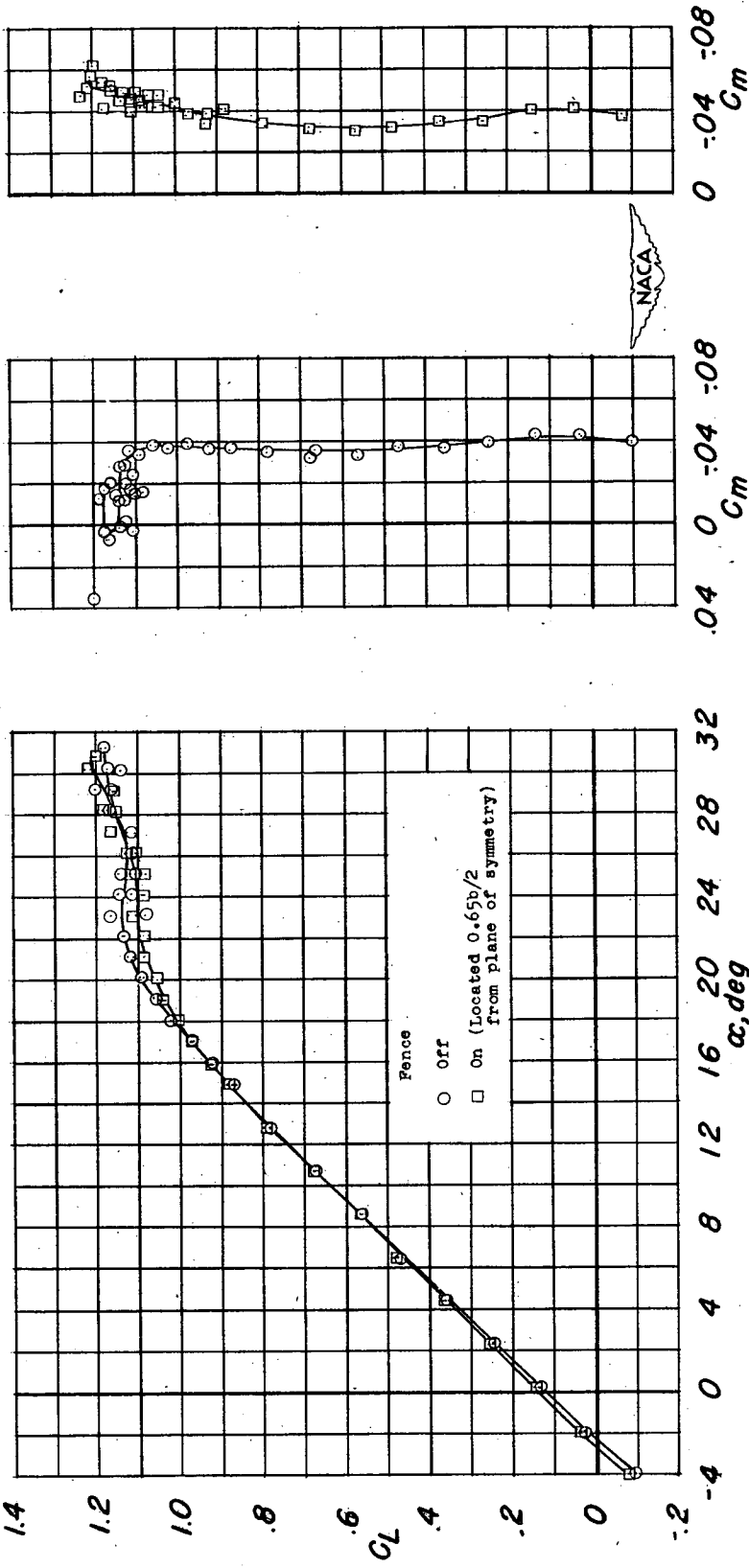
(a) Variation of C_m and α with C_L.

Figure 12.- The effect of 0.40b/2 trailing-edge flaps on the aerodynamic
characteristics of a 52° sweptback wing with 0.40b/2 extensible
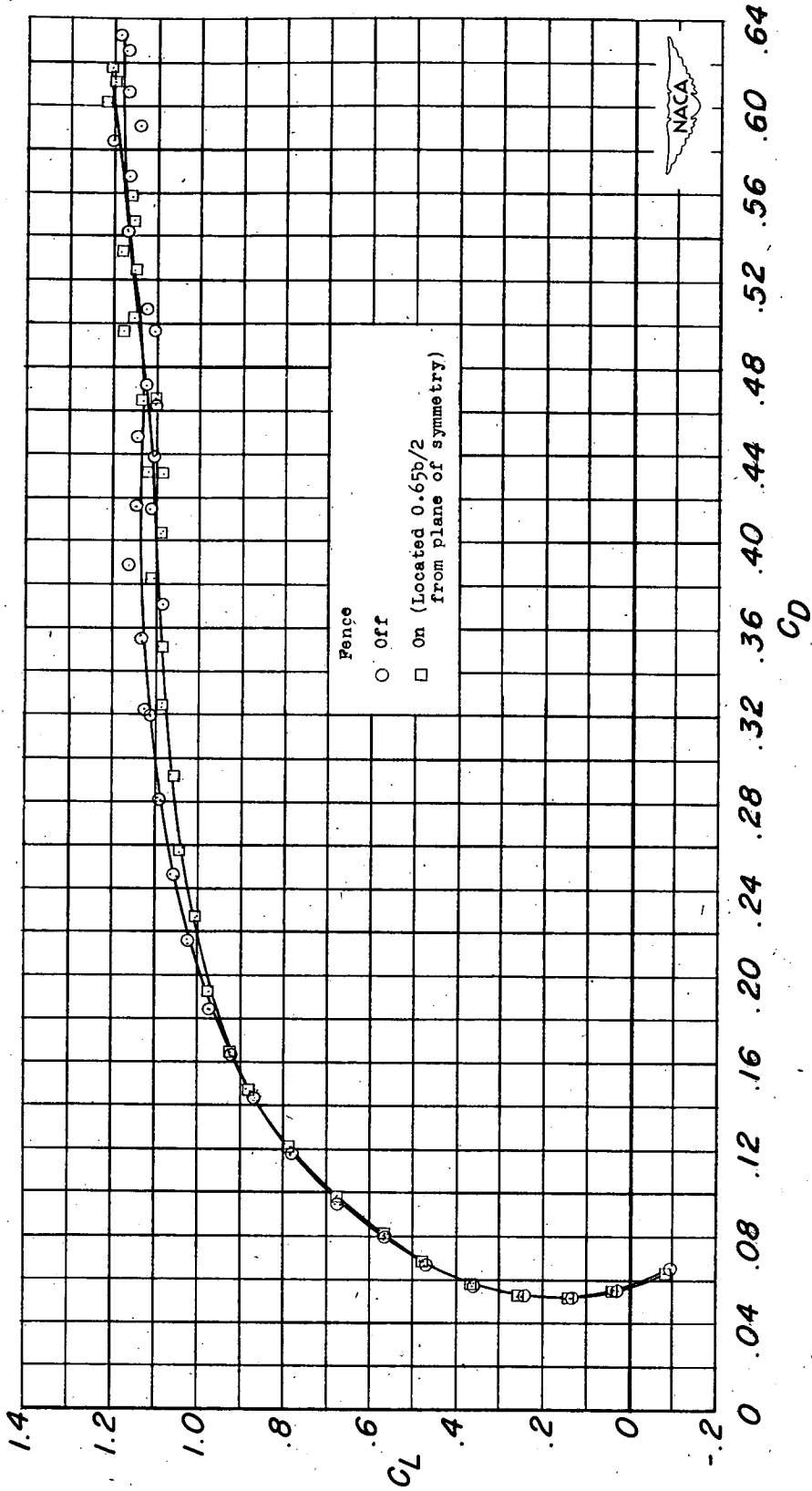leading-edge flaps and a fuselage; midwing combination. $R = 6.0 \times 10^6$.
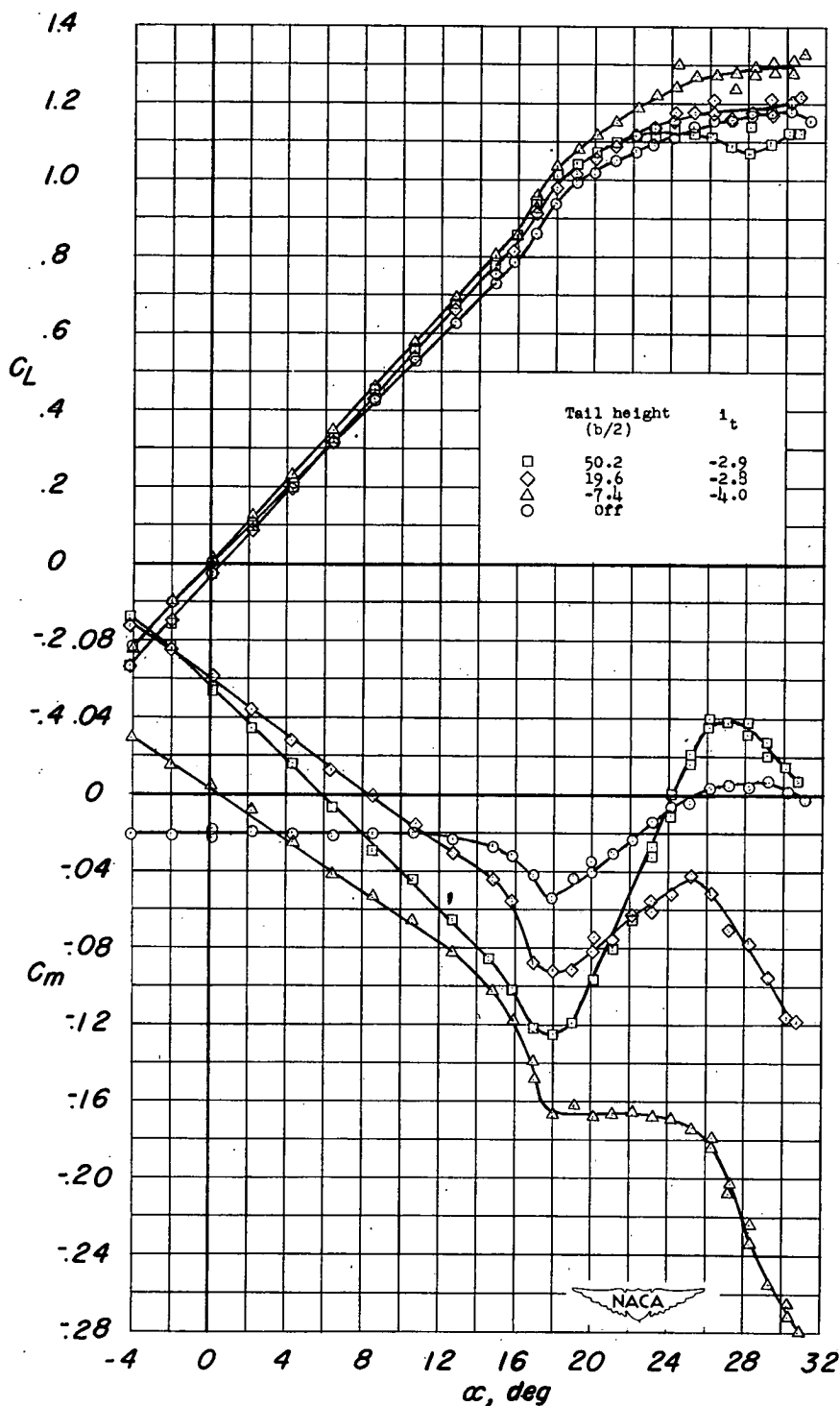
(b) Variation of C_D with C_L.

Figure 12.- Concluded.

(a) Variation of C_m and α with C_L.

Figure 13.- The effects of an upper-surface fence on the aerodynamic
characteristics of a 52° sweptback wing with 0.40b/2 extensible
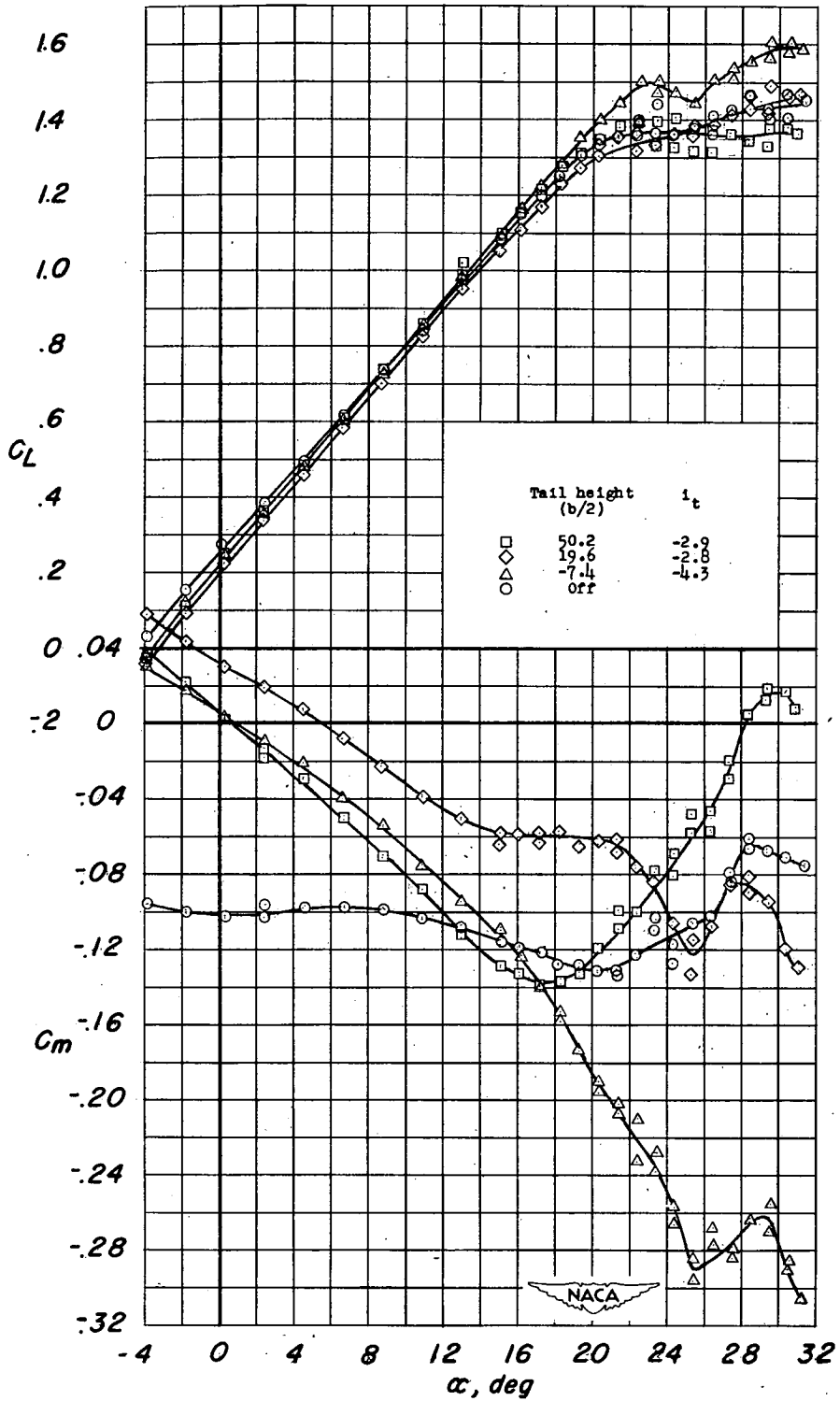leading-edge and split flaps and a fuselage; midwing combination.
R = 6.0 × 10⁶.
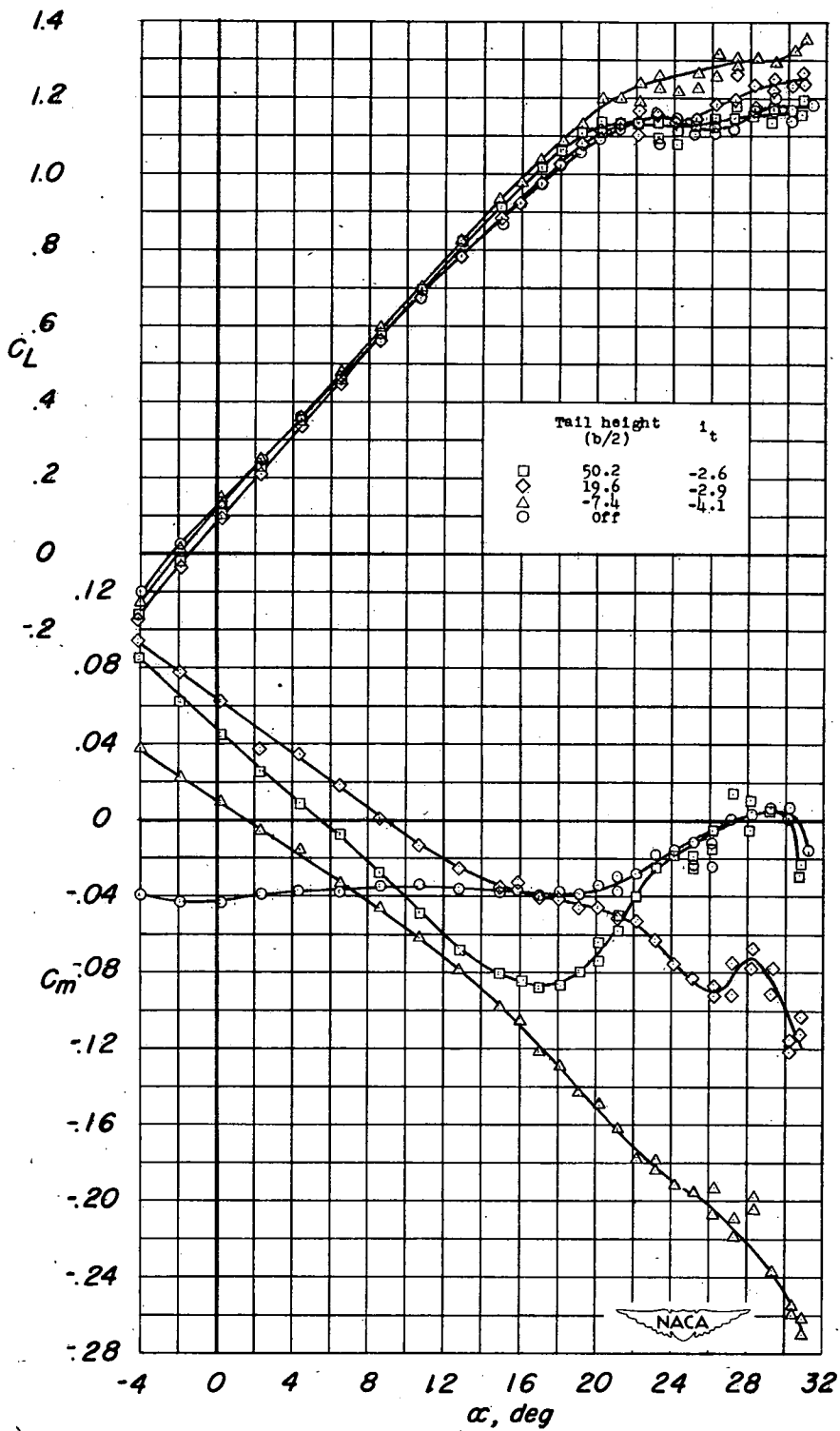
(b) C_L plotted against C_D.

Figure 13.- Concluded.

(a) Flaps off.

Figure 14.- Aerodynamic characteristics of a 52° sweptback-wing -
fuselage combination with a horizontal tail; midwing. R = 6.0 × 10⁶.

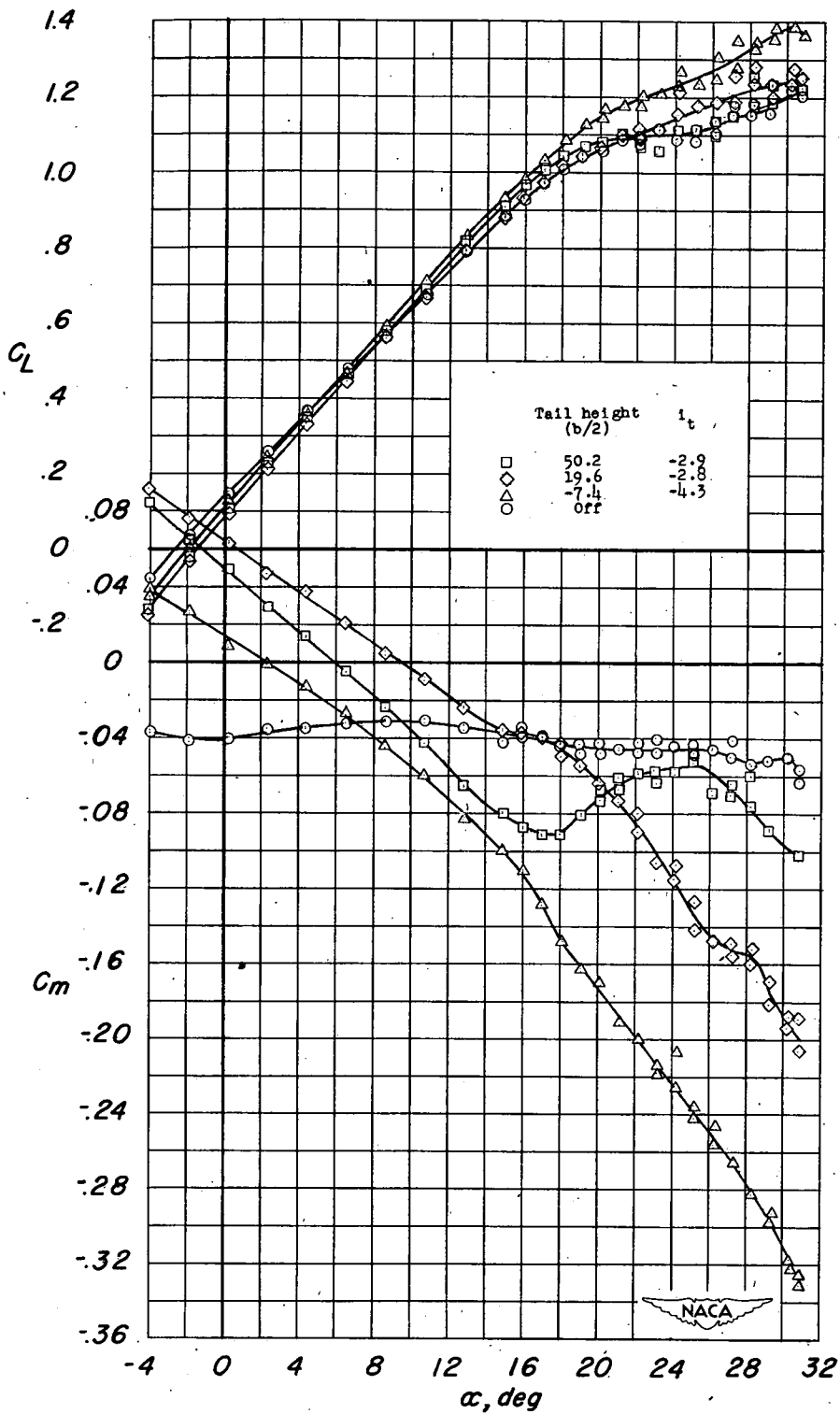Tail height i_t
(b/2)

□   50.2   -2.9
◇   19.6   -2.8
△   -7.4   -4.3
○   Off

(b) 0.40b/2 extended trailing- and leading-edge flaps.

Figure 14.- Continued.

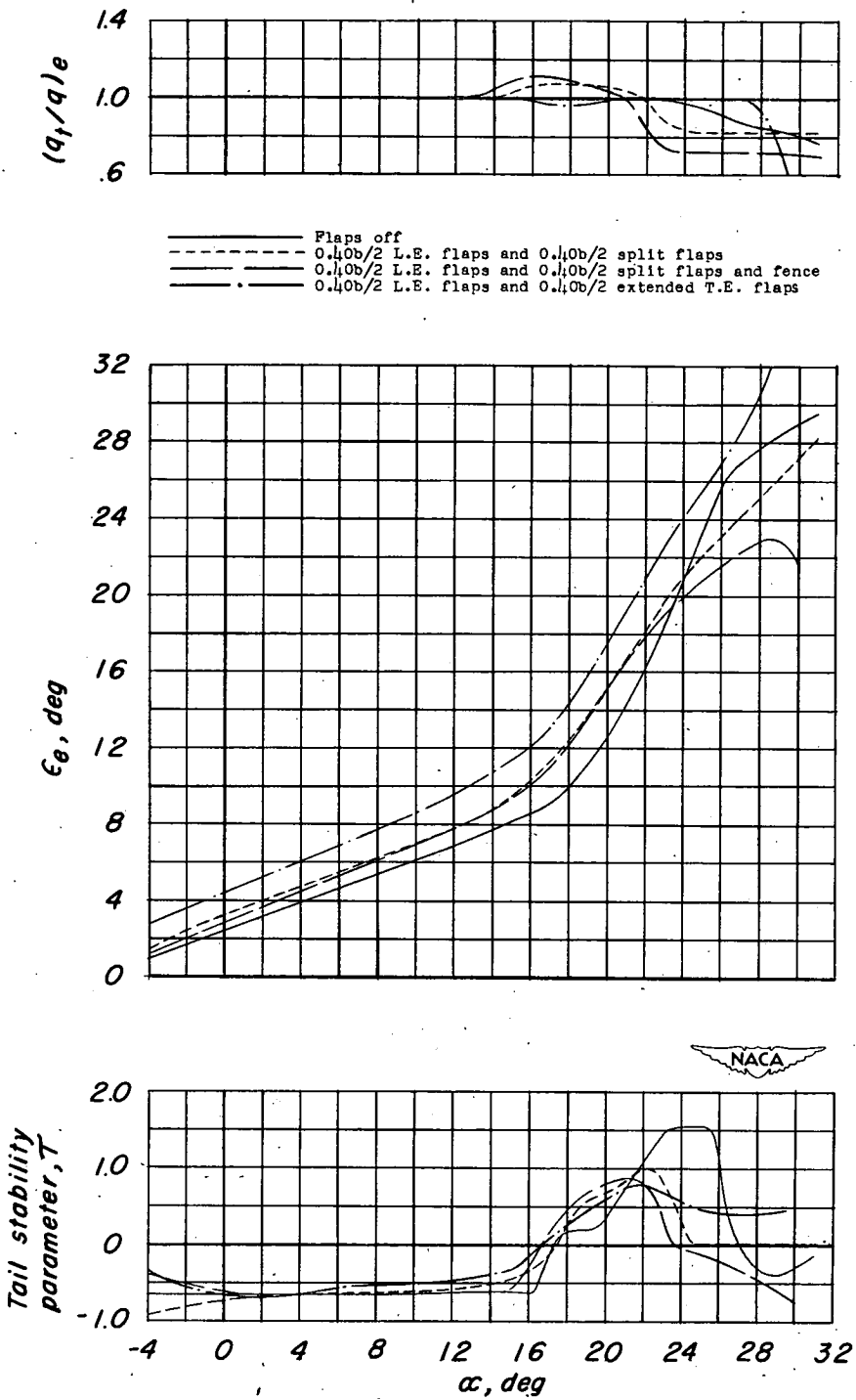| Tail height (b/2)	i_t
□ 50.2	-2.6
◇ 19.6	-2.9
△ -7.4	-4.1
○ off	

(c) 0.40b/2 split and leading-edge flaps.

Figure 14.- Continued.

(d) 0.40b/2 split and leading-edge flaps, fences at 0.65b/2.

Figure 14.- Concluded.
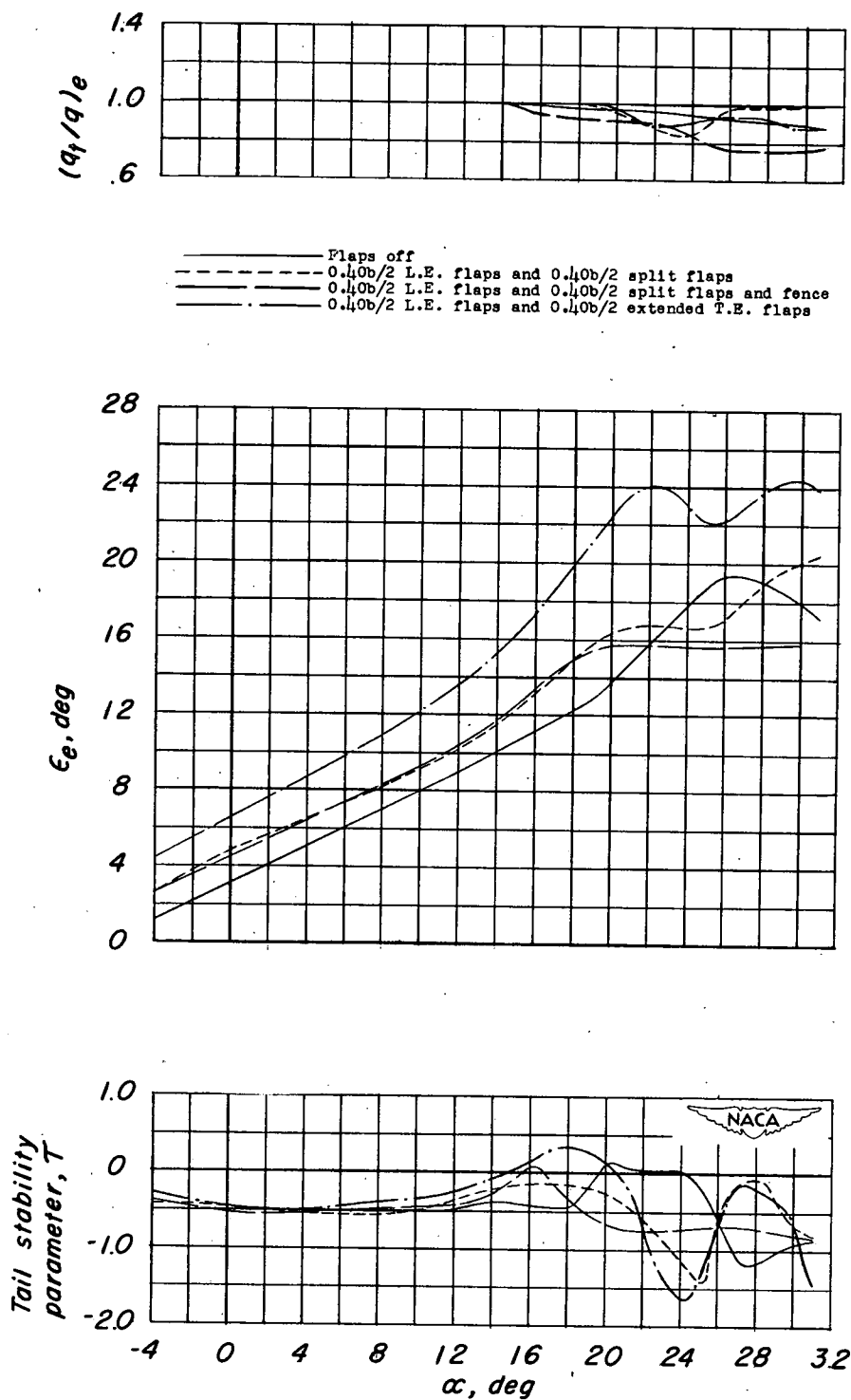
Flaps off
0.40b/2 L.E. flaps and 0.40b/2 split flaps
0.40b/2 L.E. flaps and 0.40b/2 split flaps and fence
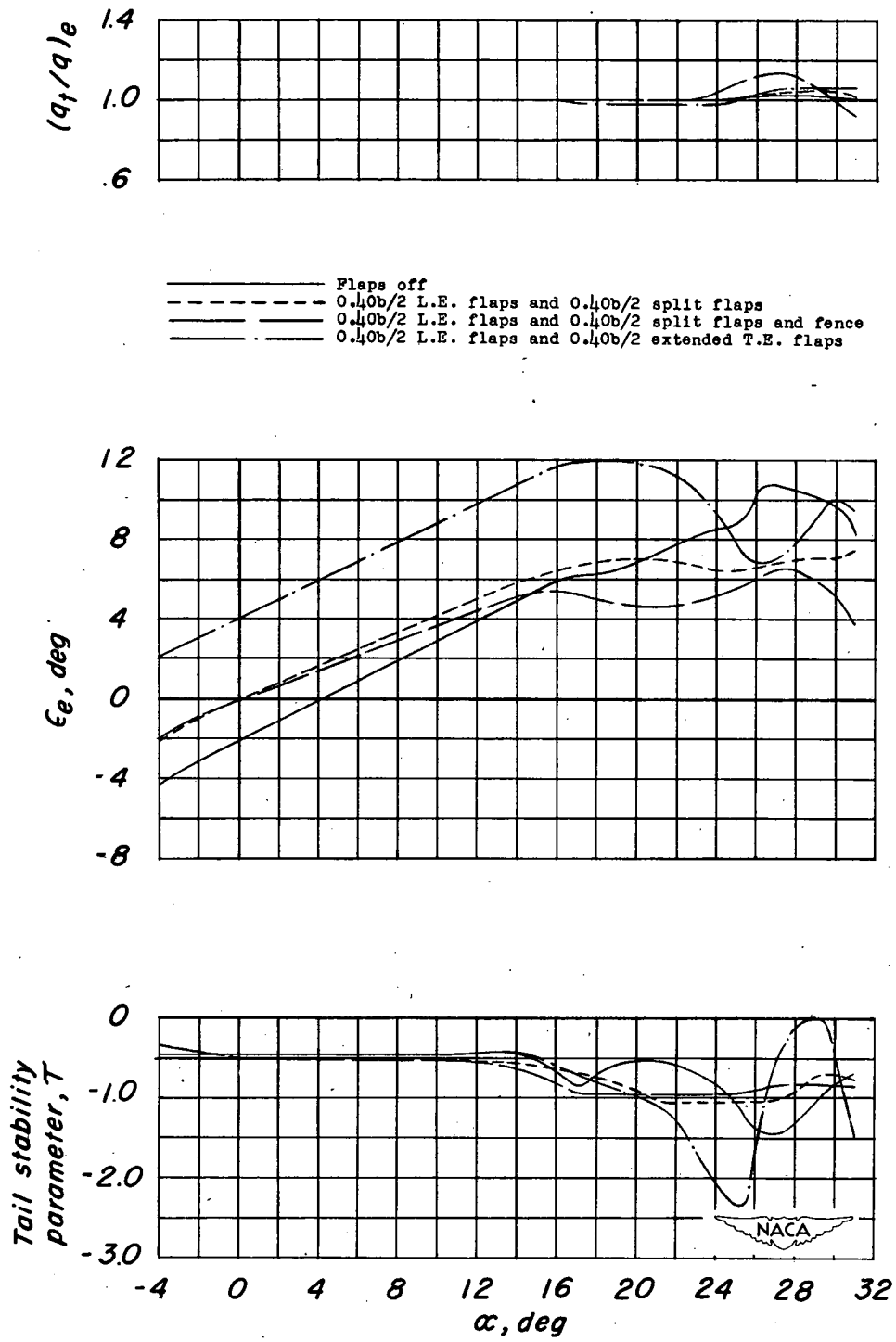0.40b/2 L.E. flaps and 0.40b/2 extended T.E. flaps

(a) Tail height, 0.504b/2.

Figure 15.- Variation of ϵ_e, $(q_t/q)_e$, and τ with angle of attack for various wing-fuselage configurations.

(b) Tail height, 0.196b/2.

Figure 15.- Continued.

(c) Tail height, -0.074b/2,

Figure 15.- Concluded.

Dynamic-pressure ratio q_t/q

Downwash angle ϵ and
sidewash angle σ in deg
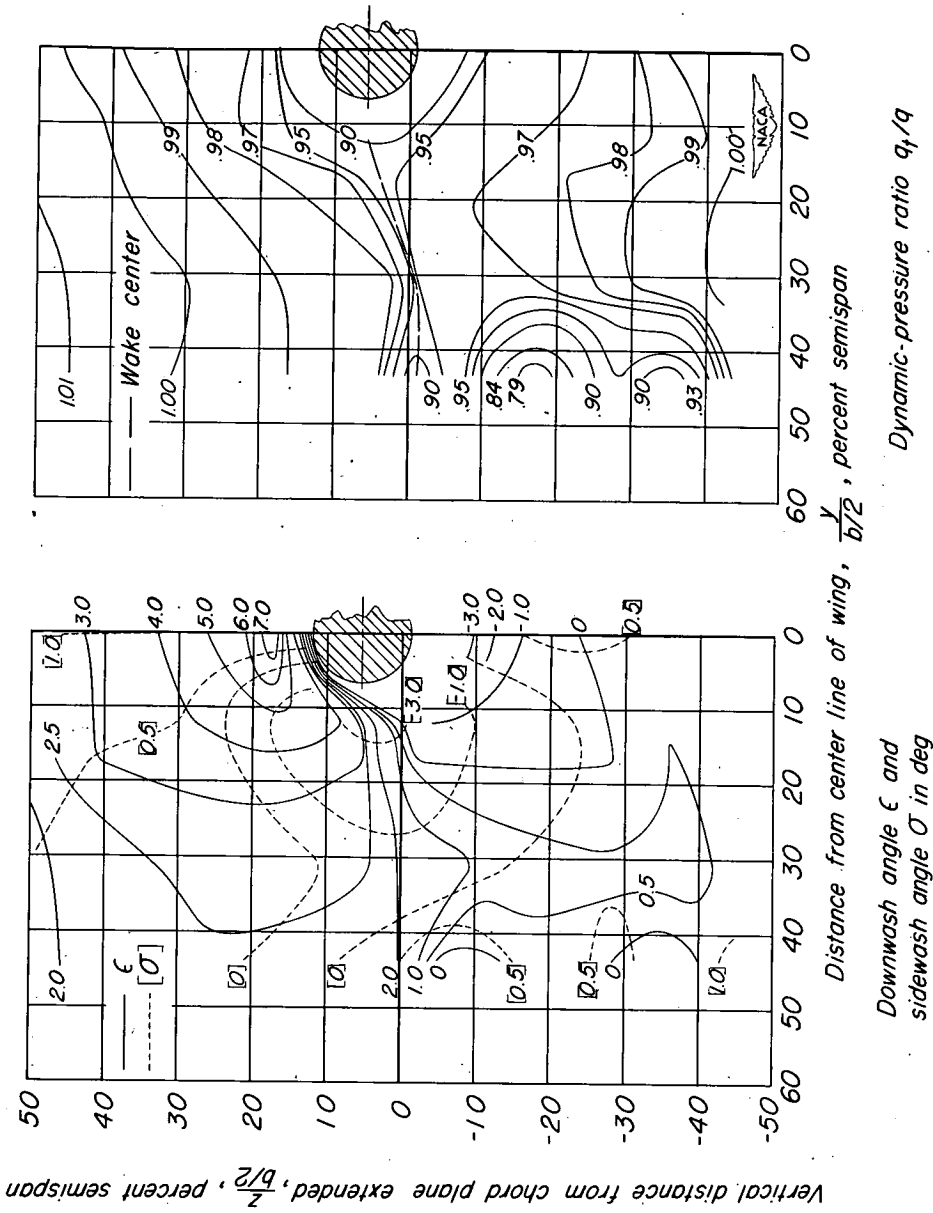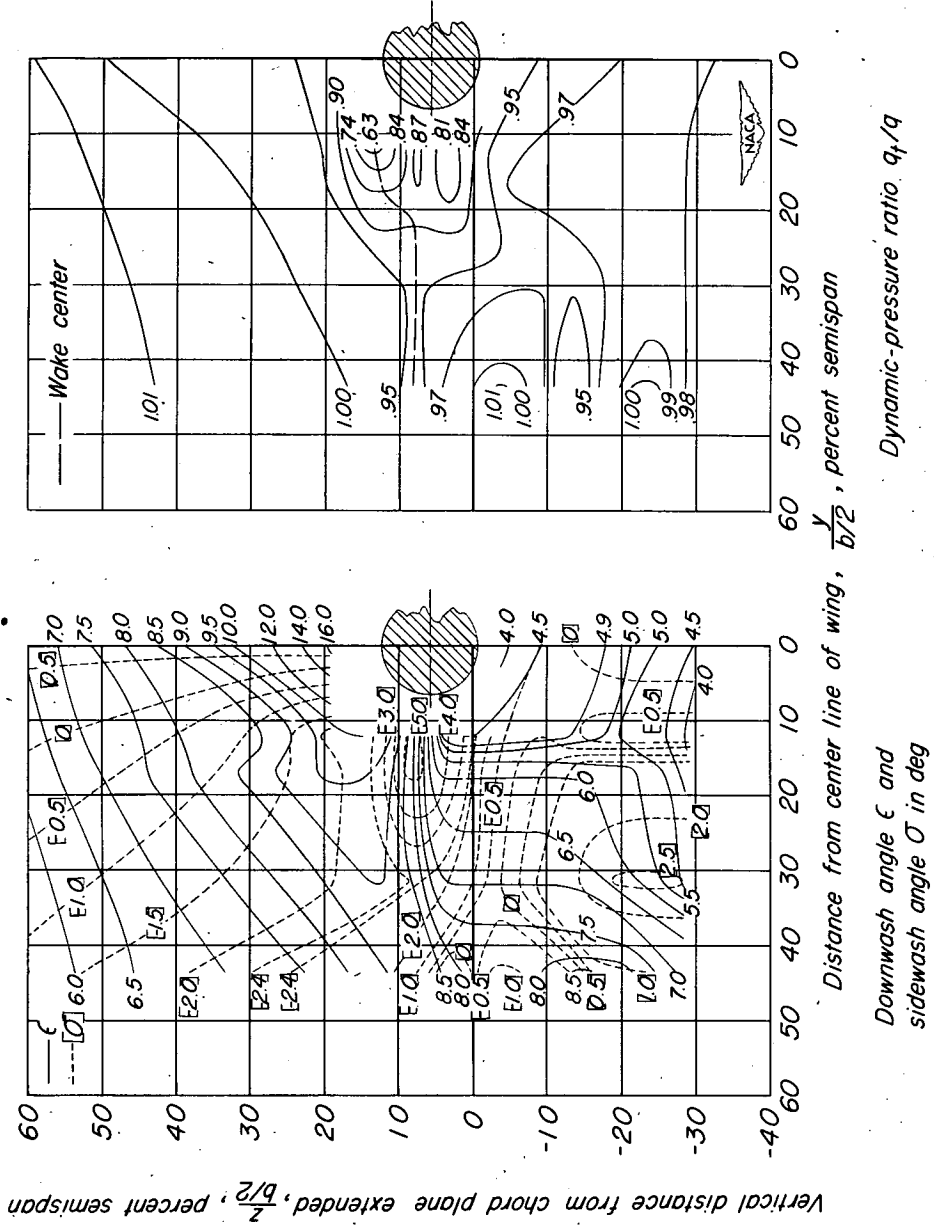
(a) $\alpha = 3.3°$.

Figure 16.- Contours of downwash, sidewash, and dynamic-pressure ratio
behind a $52°$ sweptback wing and fuselage in the region of a horizontal
tail. Flaps off; $R = 6.0 \times 10^6$.

Dynamic-pressure ratio q_t/q

Distance from center line of wing, $\frac{y}{b/2}$, percent semispan

Downwash angle ϵ and
sidewash angle σ in deg

Vertical distance from chord plane extended, $\frac{z}{b/2}$, percent semispan

(b) $\alpha = 8.1°$.

Figure 16.- Continued.

Dynamic-pressure ratio q_t/q

Downwash angle ϵ and
sidewash angle σ in deg

(c) $\alpha = 13.0°$.

Figure 16.- Continued.

Dynamic-pressure ratio q_t/q

Downwash angle ϵ and
sidewash angle σ in deg

Distance from center line of wing, $\frac{y}{b/2}$, percent semispan

Vertical distance from chord plane extended, $\frac{z}{b/2}$, percent semispan

(d) $\alpha = 16.3°$.

Figure 16.- Continued.

Distance from center line of wing, $\frac{y}{b/2}$, percent semispan

Dynamic-pressure ratio q_t/q

Downwash angle ϵ and
sidewash angle σ in deg

Vertical distance from chord plane extended, $\frac{z/2}{b/2}$, percent semispan
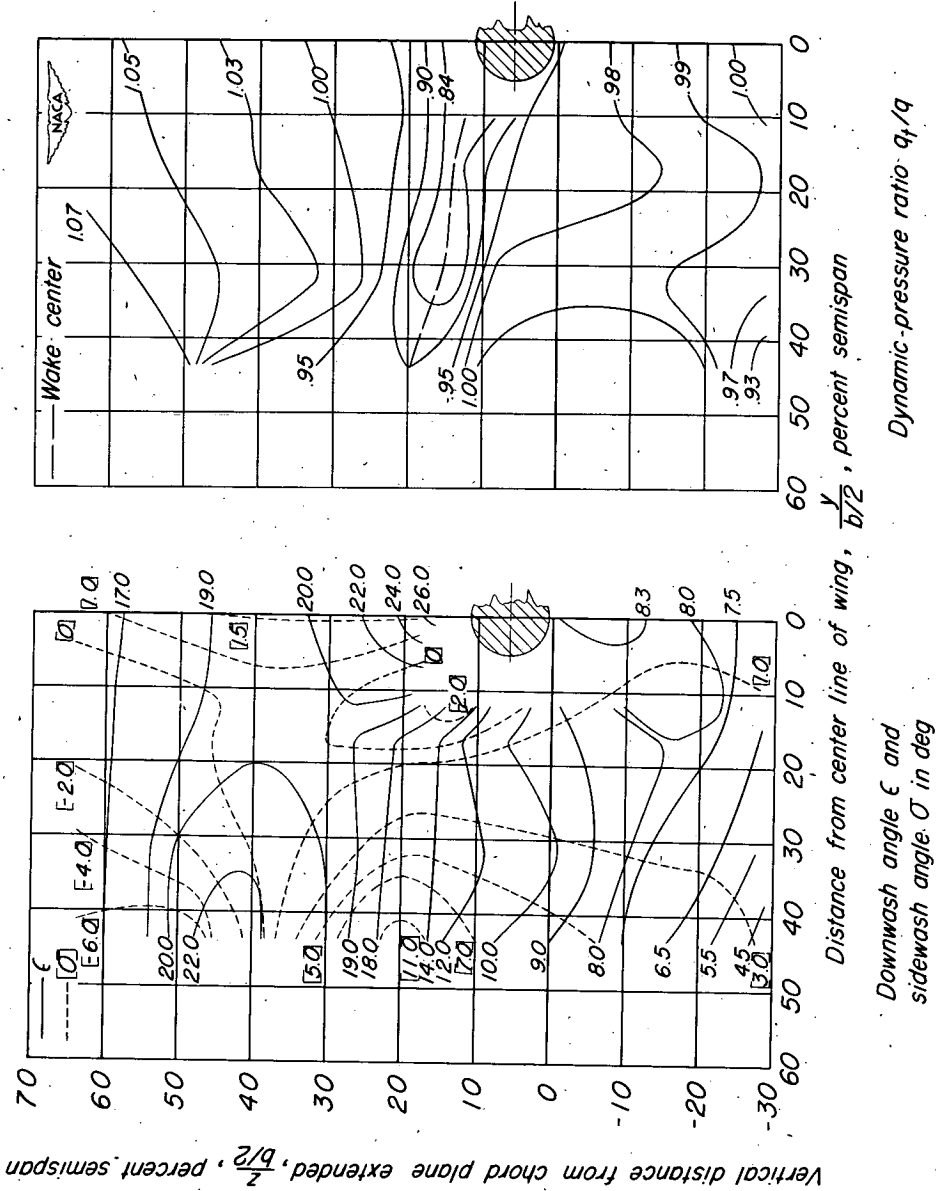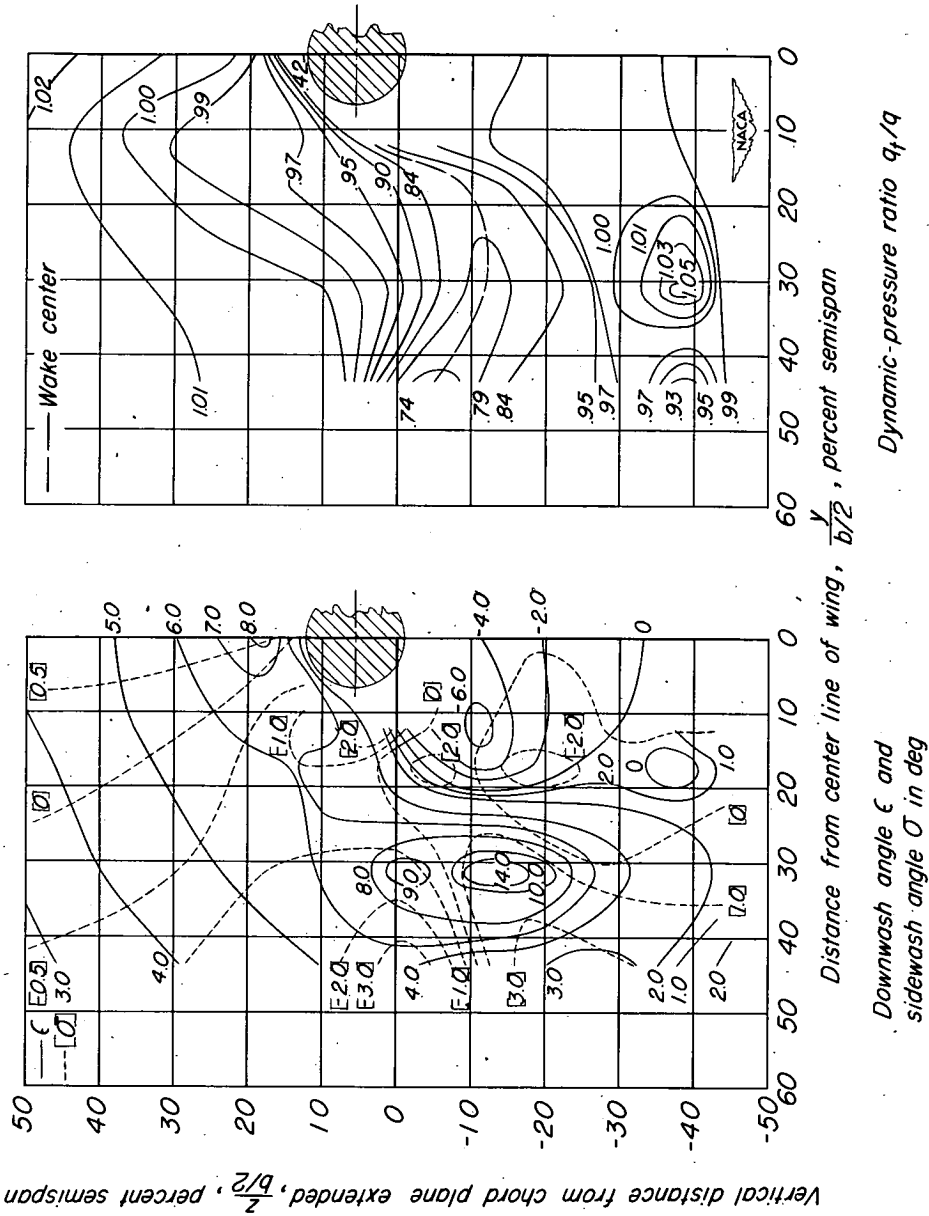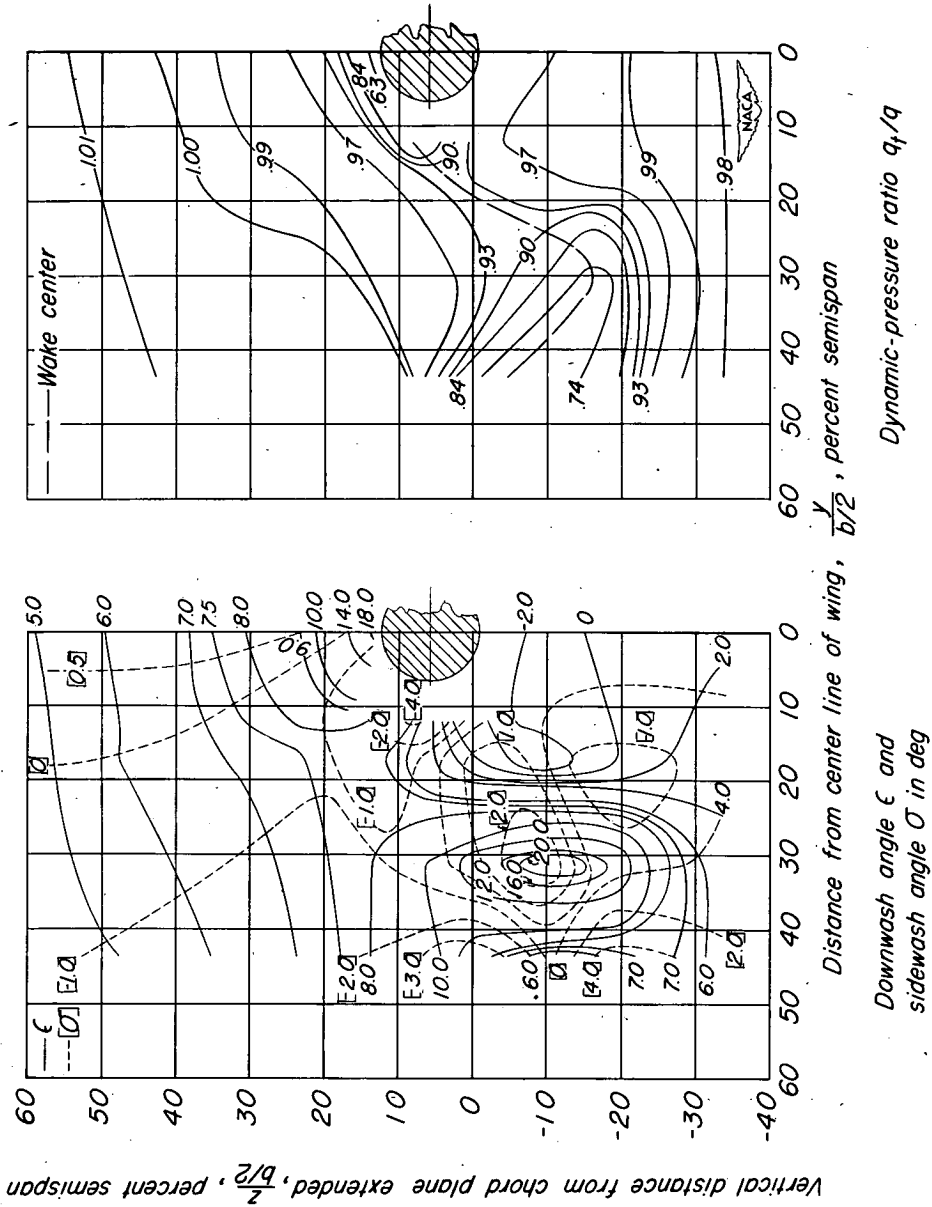
(e) $\alpha = 19.0°$.

Figure 16.- Continued.
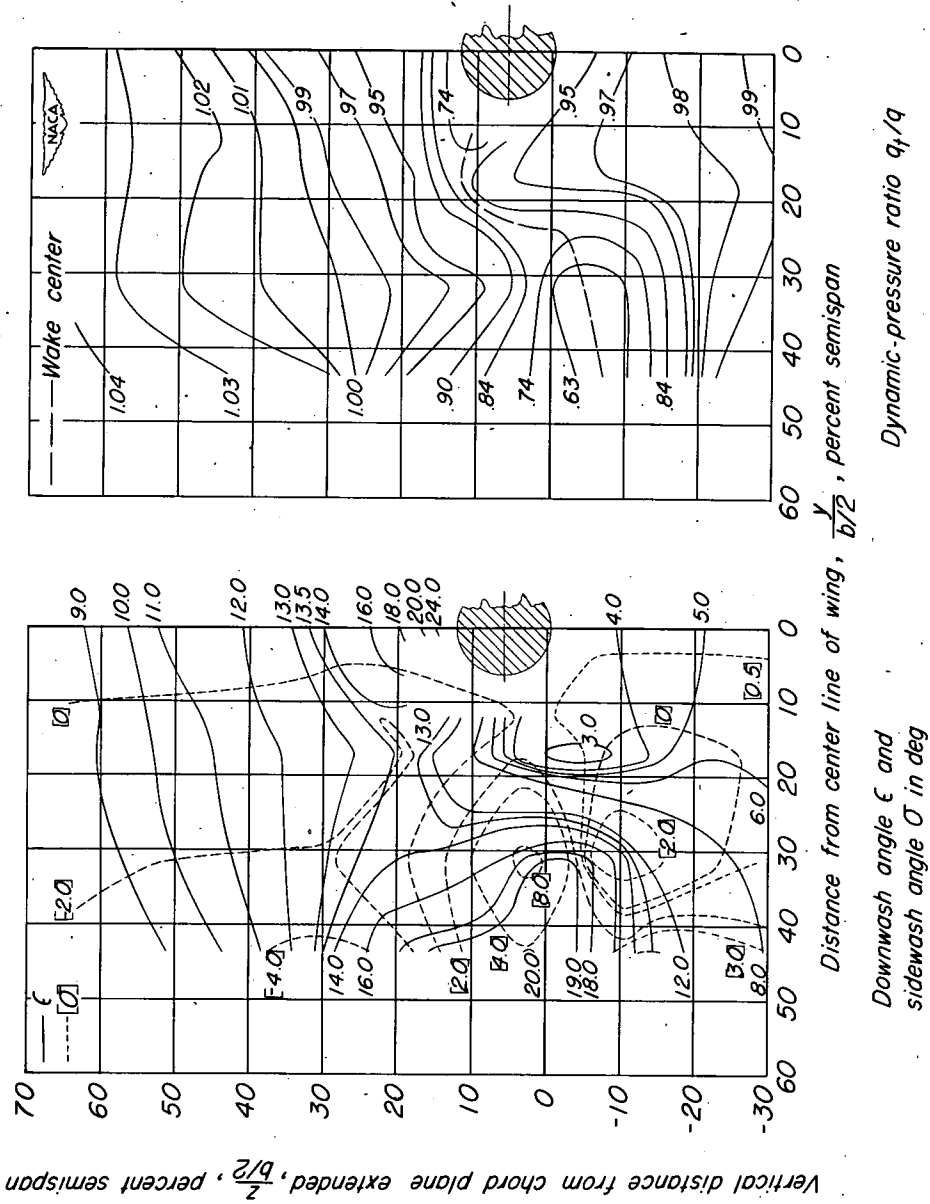
(f)   α = 23.1°.

Figure 16.- Concluded.

(a) α = 3.3°.

Figure 17.- Contours of downwash, sidewash, and dynamic-pressure ratio
behind a 52° sweptback wing and fuselage in the region of a horizontal
tail; 0.40b/2 leading-edge and split trailing-edge flaps; R = 6.0 × 10⁶.

(b) $\alpha = 8.1°$.

Figure 17.- Continued.

Dynamic-pressure ratio q_t/q

Downwash angle ϵ and
sidewash angle σ in deg

Distance from center line of wing, $\frac{y}{b/2}$, percent semispan

Vertical distance from chord plane extended, $\frac{z}{b/2}$, percent semispan

(c) $\alpha = 13.0°$.

Figure 17.- Continued.

(d)   α = 16.3°.

Figure 17.- Continued.

Distance from center line of wing, $\frac{y}{b/2}$, percent semispan

Dynamic-pressure ratio q_t/q

Downwash angle ϵ and
sidewash angle σ in deg

Vertical distance from chord plane extended, $\frac{z}{b/2}$, percent semispan

(e) $\alpha = 19.0°$.

Figure 17.- Continued.

Downwash angle ∈ and
sidewash angle σ in deg.

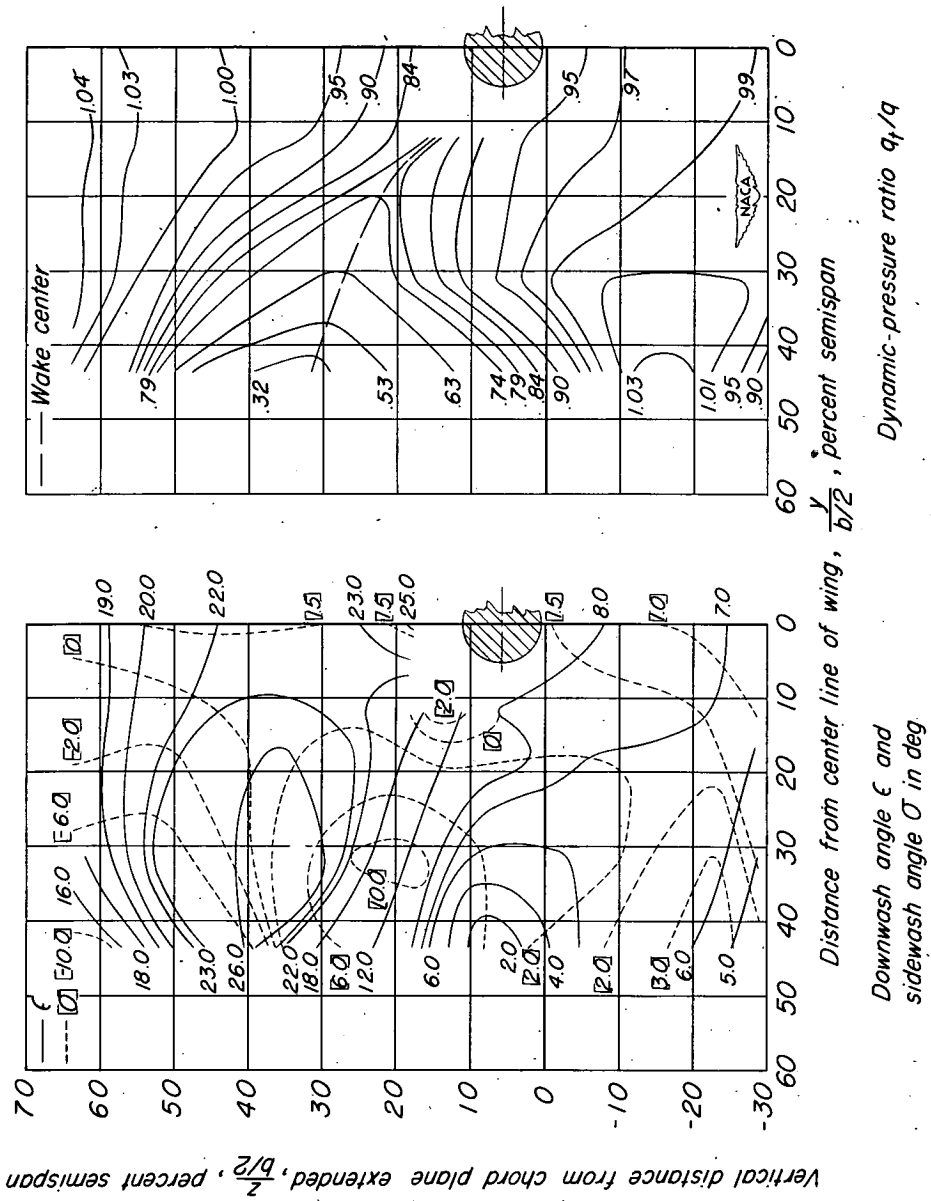Dynamic-pressure ratio q_t/q

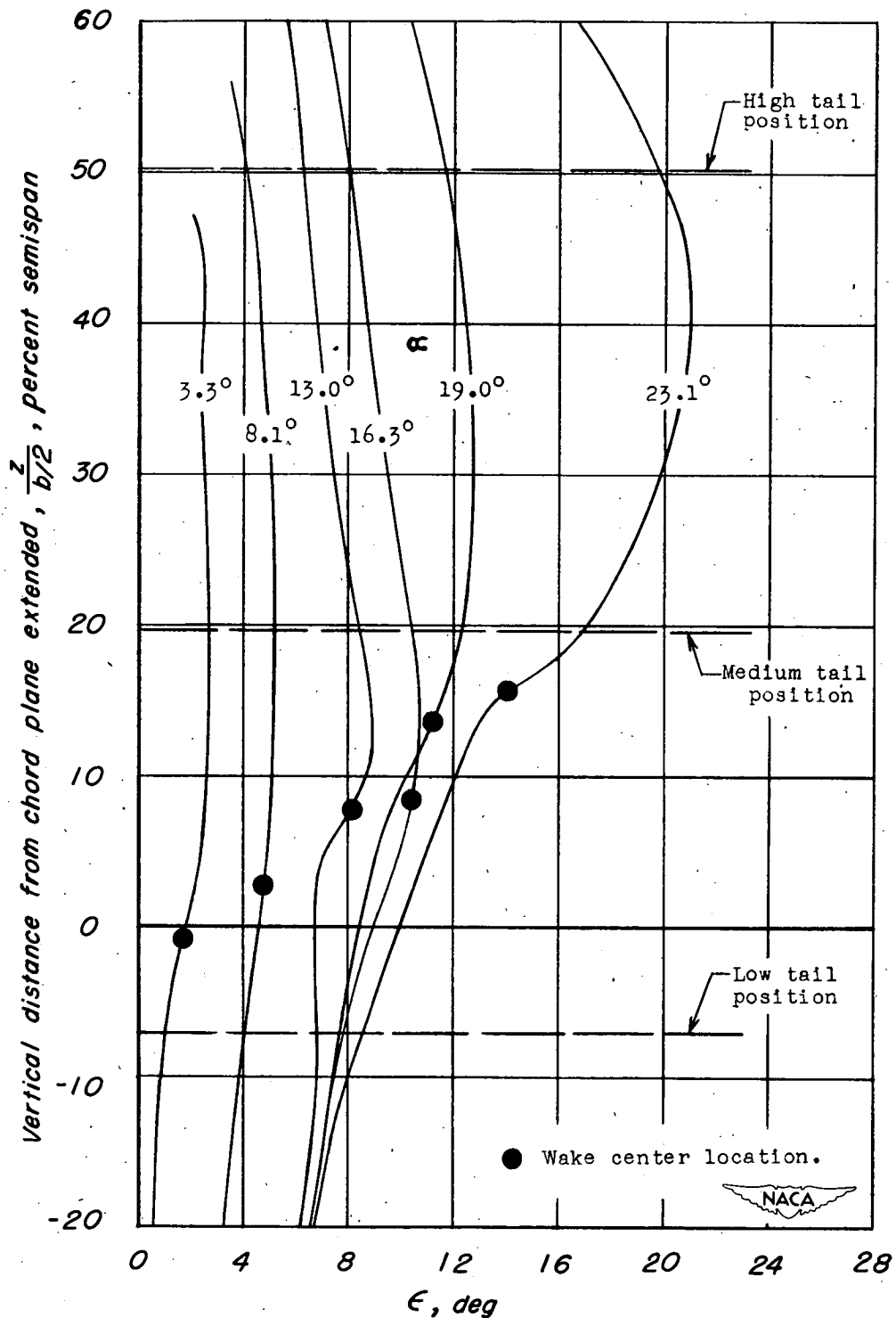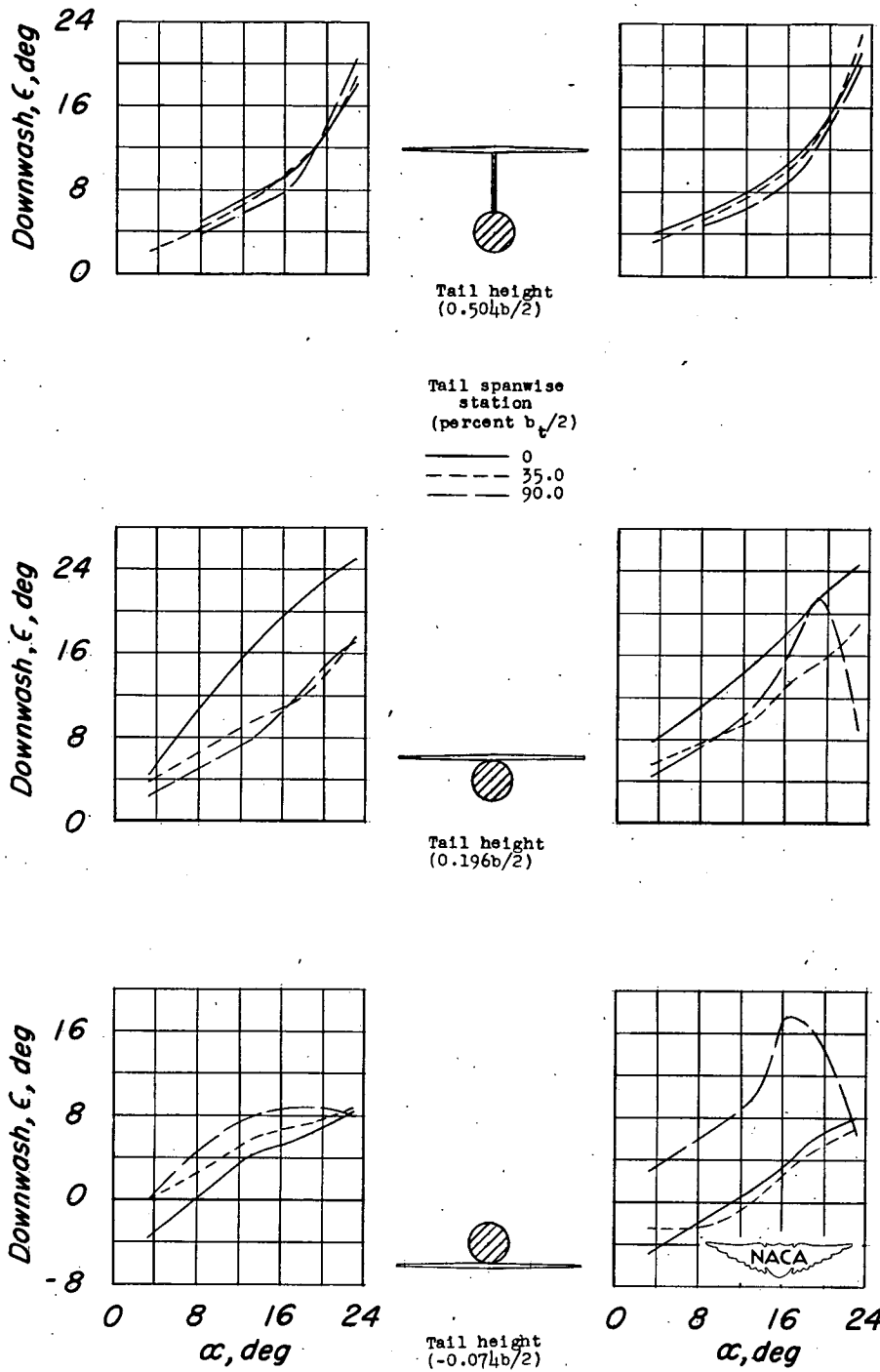(f) α = 23.1°.

Figure 17.- Concluded.

Figure 18.- Representative downwash profile and wake center location at
various angles of attack plotted against vertical distance from the
extended wing-chord plane in the vicinity where a horizontal tail
might be located; y = 0.313b/2; flaps off.

(a) Without flaps.   (b) With 0.40b/2 leading-edge and
                               split trailing-edge flaps.

Figure 19.- Variation of downwash angle at several spanwise stations of
    various tail arrangements plotted against angle of attack.

| | Λ $\bar{c}/4$ (deg) | Wing | | | Longitudinal location behind $\bar{c}/4$, percent $\bar{c}$ | Ref. |
		A	Airfoil Section	$\bar{c}$ (in.)		
◁	0	3.00	NACA 0015	10.00	172.5	10
◻	0	6.00	NACA 0015	10.00	172.5	10
▷	30	5.20	NACA 0015	11.50	172.5	10
▽	30	4.50	NACA 0015	11.50	172.5	10
▽	40	4.01	NACA 64$_1$-112	34.70	200.0	6
⊘	45	5.10	NACA 64-210	31.22	210.0	11
⊘	50	2.88	NACA 64$_1$-112	39.97	165.0	-
◻	60	3.00	NACA 0015	20.00	150.0	10
◇	60	1.50	NACA 0015	20.00	172.5	10

Note: Flagged symbols indicate mid-wing fuselage configurations.

(a) Plane of symmetry.

(b) 33.3 percent semispan from plane of symmetry.
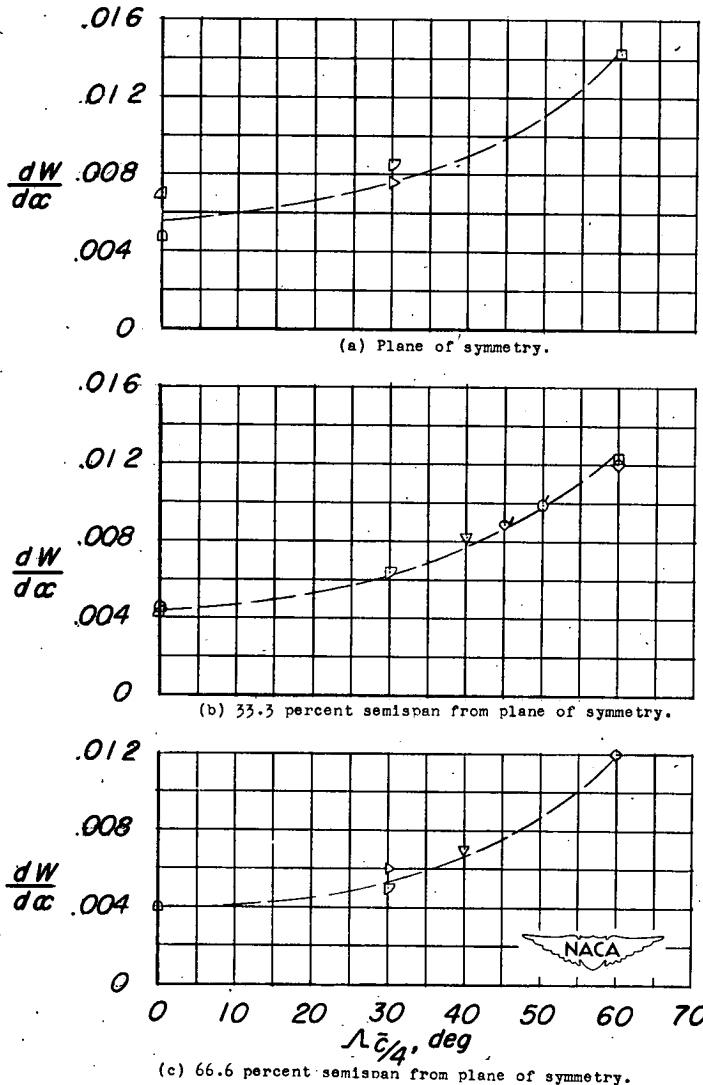
(c) 66.6 percent semispan from plane of symmetry.

Figure 20.- The rate of change of wake center location (from extended wing-chord plane) with angle of attack at several lateral stations, in the region of a horizontal tail behind wings of various plan forms, plotted against sweep angle.